University of Twente
The Netherlands

# Wave Reflection over flat and slowly varying bathymetry modeled by Effective Boundary Conditions


Wenny Kristina

Mathematical Physics and Computational Mechanics Group

Department of Applied Mathematics

Universiteit Twente


**August 2009**

# Wave reflection over flat and slowly varying bathymetry modeled by Effective Boundary Conditions

W. Kristina
Department of Applied Mathematics
Universiteit Twente

A thesis submitted for the degree of
*Master of Science (MSc)*

Supervisor: Prof. Dr. E. W. C. van Groesen

Co-supervisor: Dr. O. Bokhove

Day of the defense: 24 August 2009

# Contents

# List of Figures

# 1

# Introduction

Tsunamis, from the Japanese words *'tsu' (harbour)* and *'nami' (wave)*, are long water waves generated by offshore earthquakes, explosive volcanism near the surface of the ocean, submarine slides or a meteorite that hit the ocean. A tsunami can occur in oceans, bays, lakes or reservoirs. The characteristic feature that makes a tsunami so dangerous for the coastal area is its exceptional wavelength compared to its height. In the open ocean, even the largest tsunami rarely exceeds $0.5m$ in height. However, the spacing between tsunami wave crests can be hundreds of kilometres. These characteristics allow the tsunami waveheight to increase substantially in the last $10-20m$ depth of water before the shore. Therefore, in tsunami simulations the waveheight near the shore is the most important aspect scientists would like calculate correctly.

Unfortunately, the present-day simulation tools still cannot calculate the waveheight near the shore accurately enough. One source of inaccuracy is the interaction of the incoming waves with reflected waves from the coast. Besides, computing the details of run-up and run-down of waves on the shore is computationally very demanding and expensive since closer to the shore a finer computational resolution will be needed. Moreover, the modelling of the physical processes is bound to be rather rudimentary because many aspects of tsunami propagation, e.g. nonlinearity, dispersion, friction, etc., have to be considered.

Most of the tsunami simulations nowadays will use a fixed wall as boundary condition at the shore to simplify the problem. But this will cause inaccuracies in the

reflected waves since in fact there are run-up and run-down waves on the shore. Therefore, we will need to design boundary conditions that are able to calculate more accurate wave interactions near the shore without increasing the computational cost.

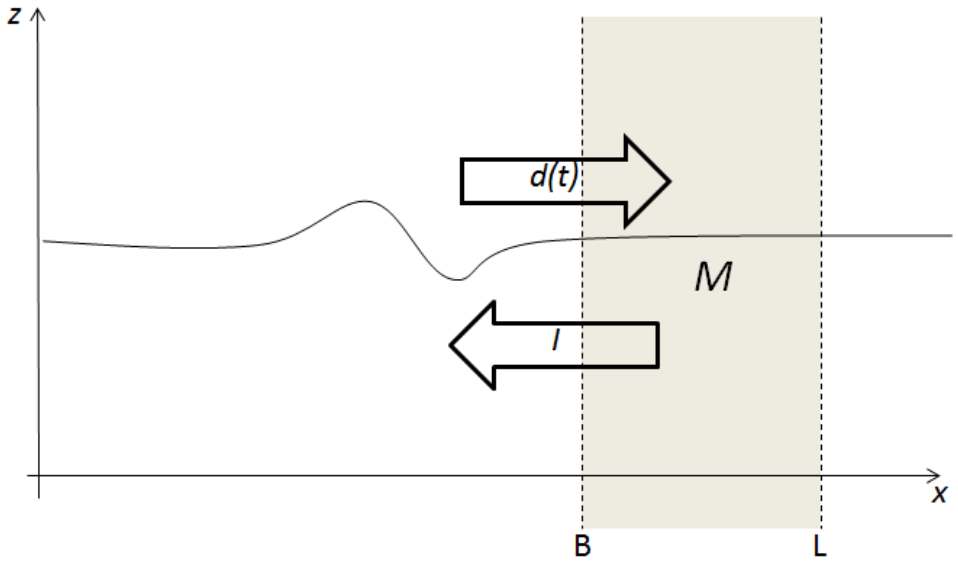


**Figure 1.1:** Effective boundary condition illustration

In this thesis, we will derive so-called Effective Boundary Conditions (EBCs) to be imposed at the shoreline. These EBCs are of general relevance and can be implemented in any numerical program to approximate the onshore tsunami flow without the necessity to calculate the detailed flooding and drying flows. The effect of the run-up of the waves on the shore when they return and interact after run-down with the incoming waves from the sea should be modeled in an approximate way in these EBCs. The illustration of the EBCs problem can be seen in fig. (1.1). In some detail, the basic idea is that in a zone before the shoreline (at a position of given, nonzero depth), $x = B$, information of the incoming wave is 'measured' in time, without disturbing the waves. Denote this information symbolically by $d(t)$. Then a theoretical model is used to obtain the wave reflection by the run-up and run-down at the shore $[B, L]$, and select the information that accounts for the reflected waves influx $I$ into the sea at the shoreline $x = B$. Symbolically this theoretical model can be denoted by $M(d)$, where

at time $t$ the result will depend on the incoming wave for all previous time, i.e.

$$I = M(d)(t) \tag{1.1}$$

depends on $d(\tau)$ for all $\tau < t$.

The challenges in this schematic overview of mapping the incoming waves to the outgoing reflected waves are:

1. Defining the 'measurement' of the property of incoming waves operator $d(t)$;
2. Making a theoretical model for the wave interaction at the shore $M(d)$;
3. Including the reflected wave properties $I = M(d)$ in an influx boundary condition; and,
4. Implementing the above analytic results numerically.

Challenges 1 and 3 are kept simple at this moment, since we model the wave propagation using linear Shallow Water Equation (SWE), which has known influx and outflux transparent boundary conditions. Actually the tsunami propagation is better modeled using a linear Variational Bousinesq Model (VBM) which will also be derived in this thesis, since it accounts the dispersive effect and vertical fluid motions. The major challenge in this thesis concerns challenge 2, in which we have to make the theoretical model for the wave interaction on the shore. Only two cases will be considered here: the EBC when the waves propagate over a flat bathymetry and are reflected by a fixed wall at $L > B$, and the EBC when the waves propagate over a slowly varying bathymetry within $[B, L]$ and continue over flat bathymetry (constant depth for $x > L$). For the numerical solution, we will use a Finite Element Method (FEM) with quadrilateral elements in two-dimensional (2D). To check the EBC, we will compare the results with the simulation on the whole domain in a one-dimensional (1D) setting.

The organization of this thesis is as follows. In Chapter 2 we will start with the derivation of the linear SWE and linear VBM from variational principles. The modeling of the EBCs over flat and slowly varying bathymetry will be described in Chapter 3 and 4. At last, conclusions and further work that is required will close this thesis in

Chapter 5. In the appendix, the numerical methods and implementations, and several test cases for linear SWE and linear VBM will be shown.

# 2

# Variational Formulation of Surface Wave

Consider the three dimensional space with two horizontal directions $\mathbf{x} = (x, y)$ and the vertical direction $z$ opposite to the direction of gravity with constant acceleration of gravity $g$. The surface elevation is denoted by $\eta(\mathbf{x}, t)$ and measured from $z = 0$. The fluid velocity is denoted by $\mathbf{U}$, with the assumption that the fluid flow is irrotational, curl $\mathbf{U} \equiv \nabla_3 \times \mathbf{U} = 0$, with $\nabla_3 = (\nabla, \partial_z)$. Hence, there exist a scalar function $\Phi$, such that $\mathbf{U} = \nabla_3 \Phi = (\nabla\Phi, \partial_z\Phi)$. The depth is given by $h(\mathbf{x}, t)$, so the bathymetry is described by $z = -h(\mathbf{x}, t)$. In this report we will assume that there is no bottom motion, so $h(\mathbf{x}, t) = h(\mathbf{x})$.

The basic equations for gravity driven irrotational motion of a layer of incompressible fluid with a free surface follow from the dynamic variational principle described by Luke's Variational Formulation (Luke 1967)

$$Crit_{\Phi,\eta} \int \mathcal{P}(\Phi, \eta) dt,$$

where

$$\mathcal{P}(\Phi, \eta) = \int [\int_{-h}^{\eta} \{\partial_t \Phi + \frac{1}{2} \mid \nabla_3 \Phi \mid^2 + gz\} dz] dx; \tag{2.1}$$

$\mathcal{P}$ is the pressure functional. Minimization of this "pressure principle" with respect to $\Phi$ gives the governing equation for the interior of the fluid, the kinematic boundary

condition at the surface and the boundary condition at the bottom. In this case, it is assumed that there is no friction and no flow through the bottom (impermeable). Minimization with respect to $\eta$ gives the dynamic free surface condition. The formulation will involve two physical quantities, i.e. $\eta(\mathbf{x},t)$ and $\phi(\mathbf{x},t) := \Phi(\mathbf{x}, z=\eta(\mathbf{x},t),t)$. The second variable is the velocity potential at the free surface.

We start with introducing $\mathcal{K}(\phi,\eta)$ as the kinetic energy functional of our basic quantities. The kinetic energy is found as the value function of the following minimization problem

$$\mathcal{K}(\phi,\eta) = \min_{\Phi}\{K(\Phi,\eta) \mid \Phi = \phi \text{ at } z=\eta\} \tag{2.2}$$

where $K(\Phi,\eta) = \int\{\int_{-h}^{\eta} \frac{1}{2} \mid \nabla_3\Phi \mid^2 dz\}d\mathbf{x}$. The functional $\mathcal{P}(\Phi,\eta)$ in (2.1) can be rewritten as

$$\mathcal{P}(\Phi,\eta) = \int[\int_{-h}^{\eta}\{\partial_t\Phi + \frac{1}{2} \mid \nabla_3\Phi \mid^2 + gz\}dz]d\mathbf{x}$$

$$= -[\int \phi\partial_t\eta d\mathbf{x} - \mathcal{K}(\Phi,\eta) - \int \frac{1}{2}g(\eta^2 - h^2)d\mathbf{x}] + \partial_t\int d\mathbf{x}\int_{-h}^{\eta}\Phi dz \tag{2.3}$$

using

$$\int_{-h}^{\eta}\partial_t\Phi dz = \partial_t\left(\int_{-h}^{\eta}\Phi dz\right) - \phi\partial_t\eta. \tag{2.4}$$

Now Luke's Variational Principle can be rewritten as follows (Miles 1977):

$$-Crit_{\phi,\eta}\int\{\int \phi\partial_t\eta d\mathbf{x} - \mathcal{H}(\phi,\eta)\}dt \tag{2.5}$$

where $\mathcal{H}(\phi,\eta)$ is the Hamiltonian Functional (total energy)

$$\mathcal{H}(\phi,\eta) = \mathcal{K}(\phi,\eta) + \int \frac{1}{2}g(\eta^2 - h^2)d\mathbf{x}. \tag{2.6}$$

The resulting variational principle in (2.5) is known as the *canonical action principle.* The Euler-Lagrange equations which are obtained by taking variations with respect to $\phi$ and $\eta$ in the action principle are given by

$$\partial_t\eta = \delta_\phi\mathcal{H}(\phi,\eta) \tag{2.7a}$$

$$\partial_t \phi = -\delta_\eta \mathcal{H}(\phi, \eta) \tag{2.7b}$$

and are known as Hamilton equations. By using (2.6), equations (2.7a)-(2.7b) can be rewritten as

$$\partial_t \eta = \delta_\phi \mathcal{H}(\phi, \eta) = \delta_\phi \mathcal{K}(\phi, \eta) \tag{2.8a}$$

$$\partial_t \phi = -\delta_\eta \mathcal{H}(\phi, \eta) = -[g\eta + \delta_\eta \mathcal{K}(\phi, \eta)]. \tag{2.8b}$$

The remaining problem is to determine the functional for the kinetic energy. The Hamiltonian containing functional $\mathcal{K}$ (2.2) can not be expressed explicitly in the basic variables $\eta$ and $\phi$, which is the essential problem of surface wave theory. Surface wave models deal with the choice of this kinetic energy, i.e. approximation for the velocity potential $\Phi$ (Cotter and Bokhove 2009, Groesen 2006, Klopman et. al. 2005). Examples of such approximation will be given in the following subsections in the form of the shallow water and Boussinesq type of approximations.

## 2.1 Shallow Water Equations

The Shallow Water Equations (SWE) are derived with the assumption that the wavelength of the waves are much larger than the depth of the fluid layer so that the vertical variations are small and will be ignored. In this case, there will be no dispersive effect. The velocity potential is approximated over depth by its value at the surface, namely $\Phi(\mathbf{x}, z, t) \approx \phi(\mathbf{x}, t)$. Thus, the kinetic energy becomes

$$\mathcal{K}(\phi, \eta) = \frac{1}{2} \int (\eta + h) \mid \nabla \phi \mid^2 d\mathbf{x}. \tag{2.9}$$

With the above approximation for kinetic energy, Luke's Variational Principle in (2.5) simplifies to

$$Crit_{\phi,\eta} \int \left[ \int \left\{ -\phi \partial_t \eta + \frac{1}{2} |\nabla \phi|^2 (\eta + h) + \frac{1}{2} g \left( \eta^2 - h^2 \right) \right\} d\mathbf{x} \right] dt. \tag{2.10}$$

The variational derivative of (2.10) with respect to $\phi$ in the direction $\delta\phi$ and with respect to $\eta$ in the direction $\delta\eta$ are

$$\int \left[ \int \left\{ -\partial_t \eta \delta\phi + (\eta + h) \nabla\phi \cdot \nabla (\delta\phi) \right\} d\mathbf{x} \right] dt = 0 \tag{2.11a}$$

$$\int \left[ \int \left\{ \partial_t \phi \delta\eta + \frac{1}{2} |\nabla\phi|^2 \delta\eta + (g\eta) \delta\eta \right\} d\mathbf{x} \right] dt = 0. \tag{2.11b}$$

The resulting Euler-Lagrange equations from the expressions in (2.11a) and (2.11b) are the non-linear SWE. Because at this moment we will use only linear SWE by restricting to waves of small amplitudes, eq.(2.11a) and eq.(2.11b) become

$$\int \left[ \int \left\{ -\partial_t \eta \delta\phi + h \nabla\phi \cdot \nabla (\delta\phi) \right\} d\mathbf{x} \right] dt = 0 \tag{2.12a}$$

$$\int \left[ \int \left\{ \partial_t \phi \delta\eta + (g\eta) \delta\eta \right\} d\mathbf{x} \right] dt = 0. \tag{2.12b}$$

The Euler-Lagrange equations lead to linear SWE

$$\partial_t \eta = -\nabla \cdot [h \nabla\phi] \tag{2.13a}$$

$$\partial_t \phi = -g\eta \tag{2.13b}$$

This system of equations (2.13a)-(2.13b) can be rewritten as one second order in time equation for $\eta$ and for $\phi$ as:

$$\partial_{tt}\eta - \nabla \cdot [c^2 \nabla\eta] = 0 \text{ or } \partial_{tt}\phi - \nabla \cdot [c^2 \nabla\phi] = 0 \tag{2.14}$$

with $c = \sqrt{gh}$.

**Finite Element Discretization of linear Shallow Water Equations.** The discretization of eq. (2.12a) and (2.12b) is obtained by approximating the unknown solution by a finite linear combination of basis functions:

$$\eta(\mathbf{x}, t) \approx \eta_h(\mathbf{x}, t) = \sum_{k=1}^{n} \widehat{\eta_k}(t) T_k(\mathbf{x}) \tag{2.15a}$$

$$\phi(\mathbf{x},t) \approx \phi_h(\mathbf{x},t) = \sum_{k=1}^{n} \widehat{\phi_k}\,(t)\, T_k\,(\mathbf{x})\,. \tag{2.15b}$$

Substitution of (2.15a)-(2.15b) in (2.12a)-(2.12b) gives

$$\int \left\{ -\left( \partial_t \sum_{k=1}^{n} \widehat{\eta_k}(t) T_k(\mathbf{x}) \right) \delta\phi + h(\mathbf{x}) \nabla \left( \sum_{k=1}^{n} \widehat{\phi_k}\,(t)\, T_k(\mathbf{x}) \right) \cdot \nabla\,(\delta\phi) \right\} d\mathbf{x} = 0 \tag{2.16a}$$

$$\int \left\{ \left( \partial_t \sum_{k=1}^{n} \widehat{\phi_k}(t) T_k(\mathbf{x}) \right) \delta\eta + g \left( \sum_{k=1}^{n} \widehat{\eta_k}\,(t)\, T_k(\mathbf{x}) \right) \delta\eta \right\} d\mathbf{x} = 0. \tag{2.16b}$$

Because $\delta\phi$ and $\delta\eta$ are arbitary admissible variations with respect to $\phi$ and $\eta$, we can also approximate these variations using the same basis function as $\delta\phi_h = \sum_{i=1}^{n} v_i T_i(\mathbf{x})$ and $\delta\eta_h = \sum_{i=1}^{n} w_i T_i(\mathbf{x})$. By substituting these approximations into (2.16a)-(2.16b), the integrals vanish for arbitrary nonzero $v$ and $w$, and we may conclude that

$$\int \left\{ -\left( \partial_t \sum_{k=1}^{n} \widehat{\eta_k}(t) T_k(\mathbf{x}) \right) T_i(\mathbf{x}) + h(\mathbf{x}) \nabla \left( \sum_{k=1}^{n} \widehat{\phi_k}\,(t)\, T_k(\mathbf{x}) \right) \cdot \nabla T_i(\mathbf{x}) \right\} d\mathbf{x} = 0 \tag{2.17a}$$

$$\int \left\{ \left( \partial_t \sum_{k=1}^{n} \widehat{\phi_k}(t) T_k(\mathbf{x}) \right) T_i(\mathbf{x}) + g \left( \sum_{k=1}^{n} \widehat{\eta_k}\,(t)\, T_k(\mathbf{x}) \right) T_i(\mathbf{x}) \right\} d\mathbf{x} = 0 \tag{2.17b}$$

for $i = 1, ..., n$.

We can rewrite the finite element discretization for linear SWE (2.17a)-(2.17b) in an algebraic ordinary differential equations system as follow:

$$\mathbf{M}\partial_t \overrightarrow{\eta} = \mathbf{G}\overrightarrow{\phi}$$

$$\mathbf{M}\partial_t \overrightarrow{\phi} = -g\mathbf{M}\overrightarrow{\eta}$$

or

$$\begin{pmatrix} \mathbf{M} & 0 \\ 0 & \mathbf{M} \end{pmatrix} \partial_t \begin{pmatrix} \overrightarrow{\eta} \\ \overrightarrow{\phi} \end{pmatrix} = \begin{pmatrix} 0 & \mathbf{G} \\ -g\mathbf{M} & 0 \end{pmatrix} \begin{pmatrix} \overrightarrow{\eta} \\ \overrightarrow{\phi} \end{pmatrix} \tag{2.18}$$

where $\overrightarrow{\eta}$ and $\overrightarrow{\phi}$ denote the vectors solution for $\eta_h$ and $\phi_h$. The entry of a matrix $\mathbf{M}$ is given by $m_{ij} = \int_\Omega T_i(\mathbf{x})T_j(\mathbf{x})d\Omega$, and the entry of a matrix $\mathbf{G}$ is given by $g_{ij} = \int_\Omega h(\mathbf{x})\nabla T_i(\mathbf{x}) \cdot \nabla T_j(\mathbf{x})d\Omega$.

## 2.2 Variational Boussinesq Model

The Variational Boussinesq Model (VBM) aims to make a better approximation for the kinetic energy that will lead to (approximate) dispersive effect. In shallow water, the velocity potential at every depth is approximated by its value at the surface, but now, the approximation for $\Phi$ will depend on $z$. Instead of minimizing the kinetic energy over all $\Phi$, we minimize it only over a subset

$$\Phi = \phi(x) + F(z)\psi(x), \quad \text{with } F(z=\eta) = 0. \tag{2.19}$$

Here the additional function $\psi$ on the surface becomes a new variable and the vertical profile function $F$ will be chosen appropriately. The choice such that $F(\eta) = 0$ is taken to assure that $\Phi(z = \eta) = \phi$. Since the choice for $\Phi(\mathbf{x}, z, t)$ is given by (2.19), the kinetic energy depends also on $\psi : K(\phi, \eta, \psi)$. From (2.2) it follows that, besides the dynamic equations we will have in addition $\delta_\psi K = 0$.

To get the functional for the kinetic energy, observe that $|\nabla_3\Phi|^2 = (\nabla\Phi)^2 + (\partial_z\Phi)^2 = [\nabla\phi + (\nabla_2\psi)\,F]^2 + (\psi F')^2$, where $F'$ denotes derivative with respect to $z$. Instead of (2.9), the kinetic energy for VBM reads

$$K(\phi,\eta) = \frac{1}{2}\int\left[\int_{-h}^{\eta}\left\{(\nabla\phi + F\nabla\psi)^2 + (F'\psi)^2\right\}dz\right]d\mathbf{x}.$$

By expanding the equation above, we get

$$K(\phi,\eta) = \frac{1}{2}\int\left[\int_{-h}^{\eta}\left\{|\nabla\phi|^2 + 2F\nabla\phi\cdot\nabla\psi + (F|\nabla\psi|)^2 + (F'\psi)^2\right\}dz\right]d\mathbf{x}.$$

Introducing the coefficients (which will depend on $\mathbf{x}$ through $\eta$ and $h$)

$$\alpha = \int_{-h}^{\eta} F^2 dz,\ \beta = \int_{-h}^{\eta} F dz,\ \gamma = \int_{-h}^{\eta}\left(F'\right)^2 dz \tag{2.20}$$

we obtain

$$K(\phi,\eta)=\frac{1}{2}\int\left\{|\nabla\phi|^2(\eta+h)+2\beta\nabla\phi\,\centerdot\,\nabla\psi+\alpha|\nabla\psi|^2+\gamma\psi^2\right\}d\mathbf{x}. \tag{2.21}$$

Now we rewrite Luke's variational principle in (2.5) in a form of a minimization problem with respect to three variables $(\phi,\eta,\psi)$

$$Crit_{\phi,\eta,\psi}\int\left\{\begin{array}{c}\int-\phi\partial_t\eta d\mathbf{x}+\frac{1}{2}\left|\nabla\phi\right|^2(\eta+h)+2\beta\nabla\phi\,\centerdot\,\nabla\psi\\+\alpha|\nabla\psi|^2+\gamma\psi^2+\frac{1}{2}g\left(\eta^2-h^2\right)\end{array}\right\}dt. \tag{2.22}$$

The variational derivative of (2.22) with respect to $\phi$, $\eta$, and $\psi$ in the direction $\delta\phi$, $\delta\eta$, and $\delta\psi$ leads to three equations below

$$\int\left[\int(\delta\phi)\,\partial_t\eta d\mathbf{x}-\int\left\{(\eta+h)\,\nabla\phi\,\centerdot\,\nabla(\delta\phi)+\beta\nabla(\delta\phi)\,\centerdot\,\nabla\psi\right\}d\mathbf{x}\right]dt=0 \tag{2.23a}$$

$$\int\left[-\int(\delta\eta)\,\partial_t\phi d\mathbf{x}-\int\left\{g\eta(\delta\eta)-\frac{1}{2}\left|\nabla\phi\right|^2(\delta\eta)\right\}d\mathbf{x}\right]dt=0 \tag{2.23b}$$

$$\int\left[\int\left\{(\beta\nabla\phi)\,\centerdot\,\nabla(\delta\psi)+(\alpha\nabla\psi)\,\centerdot\,\nabla(\delta\psi)+\gamma\psi(\delta\psi)\right\}d\mathbf{x}\right]dt=0. \tag{2.23c}$$

As we did in SWE, to simplify the problem, linearization of the variational derivatives above result in

$$\int\left[\int(\delta\phi)\,\partial_t\eta d\mathbf{x}-\int\left\{h\nabla\phi\,\centerdot\,\nabla(\delta\phi)+\beta\nabla(\delta\phi)\,\centerdot\,\nabla\psi\right\}d\mathbf{x}\right]dt=0 \tag{2.24a}$$

$$\int\left[-\int(\delta\eta)\,\partial_t\phi d\mathbf{x}-\int g\eta(\delta\eta)\,d\mathbf{x}\right]dt=0 \tag{2.24b}$$

$$\int\left[\int\left\{(\beta\nabla\phi)\,\centerdot\,\nabla(\delta\psi)+(\alpha\nabla\psi)\,\centerdot\,\nabla(\delta\psi)+\gamma\psi(\delta\psi)\right\}d\mathbf{x}\right]dt=0. \tag{2.24c}$$

Note that we have defined $\alpha,\beta,\gamma$ in (2.20). Originally, $\alpha,\beta$, and $\gamma$ are functions of $\mathbf{x}$ and $t$ (through $\eta$ and $h$), but we assume now that the depth $h$ is much larger than the elevation $\eta$. So we approximate $\alpha,\beta,\gamma$ by

$$\alpha = \int_{-h}^{0} F^2 dz,\ \beta = \int_{-h}^{0} F dz,\ \gamma = \int_{-h}^{0} \left(F'\right)^2 dz.$$

The equations of linear VBM will be found from the Euler-Lagrange of the equations (2.24a)-(2.24c) as

$$\partial_t \eta = -\nabla \cdot (h\nabla\phi) - \nabla \cdot (\beta\nabla\psi) \tag{2.25a}$$

$$\partial_t \phi = -g\eta \tag{2.25b}$$

$$0 = -\nabla \cdot (\beta\nabla\phi) - \nabla \cdot (\alpha\nabla\psi) + \gamma\psi. \tag{2.25c}$$

The three coupled linear VBM equations in (2.25a)-(2.25c) have to be solved together. Given $h(\mathbf{x})$, the values of $\alpha, \beta, \gamma$ in linear VBM can be calculated beforehand. In a time stepping procedure, the algorithm is as follows. At a specific moment we have current values of $h, \eta, \phi, \psi$. To procees one time step, to arrive at $\eta^+, \phi^+, \psi^+$, the following steps have to be taken.

(1) To update the value of $\psi$ we proceed with the current $\eta$ and $\phi$, and calculate the solution $\psi^+$ of the elliptic equation

(2) Having found the updated $\psi^+$, make a time step to get updated $\eta^+, \phi^+$ from the dynamic equations

(3) Repeat the process for next time step.

In this report, the choice for the function $F(z)$ will be taken to be a parabolic profile:

$$F = \frac{2z}{h} + \frac{z^2}{h^2}. \tag{2.26}$$

This is motivated by the fact that the solution of $\Phi$ for harmonic solutions of linear wave approximation (small variation in surface elevation and mildly sloping topography) are *cosine* hyperbolic functions, which resemble a parabolic profile. Then the values of $\alpha, \beta, \gamma$ are

$$\alpha(\mathbf{x}) = \frac{8}{15} h(\mathbf{x}),\quad \beta(\mathbf{x}) = -\frac{2}{3} h(\mathbf{x}),\quad \gamma(\mathbf{x}) = \frac{4}{3h(\mathbf{x})}. \tag{2.27}$$

**Finite Element Discretization of linear Variational Boussinesq Model.** The discretization of eq. (2.24a)-(2.24c) is obtained by approximating the unknown solution by a finite linear combination of basis functions:

$$\eta(\mathbf{x},t) \approx \eta_h(\mathbf{x},t) = \sum_{k=1}^{n} \widehat{\eta_k}\,(t)\, T_k\,(\mathbf{x}) \tag{2.28a}$$

$$\phi(\mathbf{x},t) \approx \phi_h(\mathbf{x},t) = \sum_{k=1}^{n} \widehat{\phi_k}\,(t)\, T_k\,(\mathbf{x}) \tag{2.28b}$$

$$\psi\,(\mathbf{x},t) \approx \psi_h\,(\mathbf{x},t) = \sum_{k=1}^{n} \overset{\wedge}{\psi}_k\,(t)\, T_k\,(\mathbf{x})\,. \tag{2.28c}$$

As we did in the FEM implementation for SWE, we will also use the variational principle for VBM. So, we substitute the approximation for the variables $\phi, \eta$, and $\psi$ into the linear VBM in integral form (2.24a), (2.24b), and (2.24c). Then we get

$$\int \left\{ \begin{array}{c} \partial_t \left( \sum_{k=1}^{n} \overset{\wedge}{\eta}_k(t) T_k(\mathbf{x}) \right) \delta\phi \\ -h(\mathbf{x}) \nabla \left( \sum_{k=1}^{n} \overset{\wedge}{\phi}_k(t) T_k(\mathbf{x}) \right) \cdot \nabla\,(\delta\phi) \\ -\beta(\mathbf{x}) \nabla \left( \sum_{k=1}^{n} \overset{\wedge}{\psi}_k(t) T_k(\mathbf{x}) \right) \cdot \nabla(\delta\phi) \end{array} \right\} d\mathbf{x} = 0 \tag{2.29a}$$

$$\int \left\{ \partial_t \left( \sum_{k=1}^{n} \overset{\wedge}{\phi}_k(t) T_k\,(\mathbf{x}) \right) \delta\eta + g \left( \sum_{k=1}^{n} \overset{\wedge}{\eta}_k(t) T_k(\mathbf{x}) \right) \delta\eta \right\} d\mathbf{x} = 0 \tag{2.29b}$$

$$\int \left\{ \begin{array}{c} \beta(\mathbf{x}) \nabla \left( \sum_{k=1}^{n} \overset{\wedge}{\phi}_k T_k\,(\mathbf{x}) \right) \cdot \nabla\,(\delta\psi) \\ +\alpha(\mathbf{x}) \nabla \left( \sum_{k=1}^{n} \overset{\wedge}{\psi}_k T_k\,(\mathbf{x}) \right) \cdot \nabla\,(\delta\psi) \\ +\gamma\,(\mathbf{x}) \left( \sum_{k=1}^{n} \overset{\wedge}{\psi}_k T_k(\mathbf{x}) \right) (\delta\psi) \end{array} \right\} d\mathbf{x} = 0. \tag{2.29c}$$

Because $\delta\phi, \delta\eta$, and $\delta\psi$ are arbitrary admissible variations with respect to $\phi, \eta$, and $\psi$, then we can also approximate these variations using the same basis function as $\delta\phi_h = \sum_{i=1}^{n} p_i T_i(\mathbf{x})$, $\delta\eta_h = \sum_{i=1}^{n} q_i T_i(\mathbf{x})$, and $\delta\psi_h = \sum_{i=1}^{n} r_i T_i(\mathbf{x})$. If we substitute these approximation into (2.29a)-(2.29c) then the integrals vanish for arbitrary nonzero

$p, q$, and $r$; we may conclude that

$$\int \left\{ \begin{array}{c} \partial_t \left( \sum_{k=1}^{n} \overset{\wedge}{\eta_k}(t) T_k(\mathbf{x}) \right) T_i(\mathbf{x}) \\ -h(\mathbf{x}) \nabla \left( \sum_{k=1}^{n} \overset{\wedge}{\phi_k}(t) T_k(\mathbf{x}) \right) \cdot \nabla T_i(\mathbf{x}) \\ -\beta(\mathbf{x}) \nabla \left( \sum_{k=1}^{n} \overset{\wedge}{\psi_k}(t) T_k(\mathbf{x}) \right) \cdot \nabla T_i(\mathbf{x}) \end{array} \right\} d\mathbf{x} = 0 \tag{2.30a}$$

$$\int \left\{ \partial_t \left( \sum_{k=1}^{n} \overset{\wedge}{\phi_k}(t) T_k(\mathbf{x}) \right) T_i(\mathbf{x}) + g \left( \sum_{k=1}^{n} \overset{\wedge}{\eta_k}(t) T_k(\mathbf{x}) \right) T_i(\mathbf{x}) \right\} d\mathbf{x} = 0 \tag{2.30b}$$

$$\int \left\{ \begin{array}{c} \beta(\mathbf{x}) \nabla \left( \sum_{k=1}^{n} \overset{\wedge}{\phi_k} T_k(\mathbf{x}) \right) \cdot \nabla T_i(\mathbf{x}) \\ +\alpha(\mathbf{x}) \nabla \left( \sum_{k=1}^{n} \overset{\wedge}{\psi_k} T_k(\mathbf{x}) \right) \cdot \nabla T_i(\mathbf{x}) \\ +\gamma(\mathbf{x}) \left( \sum_{k=1}^{n} \overset{\wedge}{\psi_k} T_k(\mathbf{x}) \right) T_i(\mathbf{x}) \end{array} \right\} d\mathbf{x} = 0 \tag{2.30c}$$

for $i = 1, ..., n$.

We can rewrite the finite element discretization for linear VBM (2.30a)-(2.30c) in an algebraic ordinary differential equations system as follow:

$$\begin{aligned} \mathbf{M} \partial_t \overrightarrow{\eta} &= \mathbf{G} \overrightarrow{\phi} + \mathbf{R} \overrightarrow{\psi} \\ \mathbf{M} \partial_t \overrightarrow{\phi} &= -g \mathbf{M} \overrightarrow{\eta} \\ \mathbf{L} \overrightarrow{\psi} &= \mathbf{R} \overrightarrow{\phi}. \end{aligned}$$

where $\overrightarrow{\eta}$, $\overrightarrow{\phi}$, and $\overrightarrow{\psi}$ denote the vectors solution for $\eta_h$, $\phi_h$, and $\psi_h$.

The first two dynamic equations can be rewritten as a system of ordinary differential equations

$$\begin{pmatrix} \mathbf{M} & 0 \\ 0 & \mathbf{M} \end{pmatrix} \partial_t \begin{pmatrix} \overrightarrow{\eta} \\ \overrightarrow{\phi} \end{pmatrix} = \begin{pmatrix} 0 & \mathbf{G} \\ -g\mathbf{M} & 0 \end{pmatrix} \begin{pmatrix} \overrightarrow{\eta} \\ \overrightarrow{\phi} \end{pmatrix} + \begin{pmatrix} \mathbf{R} \overrightarrow{\psi} \\ 0 \end{pmatrix} \tag{2.31}$$

and the third equation can be expressed as

$$\overrightarrow{\psi} = \mathbf{L}^{-1} \left( \mathbf{R} \overrightarrow{\phi} \right) \tag{2.32}$$

The system (2.31) and (2.32) should be solved together with the algorithm described before. The entry of a matrix $\mathbf{L}$ is given by $l_{ij} = \int_\Omega -\alpha(\mathbf{x})\nabla T_i(\mathbf{x}) \cdot \nabla T_j(\mathbf{x}) - \gamma(\mathbf{x})T_i(\mathbf{x})T_j(\mathbf{x})d\Omega$, and the entry of a matrix $\mathbf{R}$ is given by $r_{ij} = \int_\Omega \beta(\mathbf{x})\nabla T_i(\mathbf{x}) \cdot \nabla T_j(\mathbf{x})d\Omega$.

# 3

# Effective Boundary Condition over Flat Bathymetry

In this chapter, we will derive the Effective Boundary Condition (EBC) for waves propagating over a flat bathymetry and reflected by a fixed wall. The challenges in deriving EBC (in Chapter 1) for this case will be answered. Challenges 1, 2, and 3 will be explained in Section 3.2, and challenge 4 in Section 3.3.

## 3.1 Problem Formulation

The physical domain from $x = 0$ until $x = L$ will be divided into two parts, as illustrated in fig. (3.1). The domain $[0, B]$ will be calculated numerically, but the domain $[B, L]$ will be calculated analytically. Note that the position $B$ will become the 'boundary' of the numerical domain, but it is not a physical boundary of any kind: the aim will be to simulate on $[0, B]$ the actual wave propagation in the physical domain $[0, L]$. Ideally, the modelling in $[B, L]$ should be so good and so well constructed at $x = B$ that there is no affect in $[0, B]$ of this hybrid analytic-numerical. The boundary at $x = 0$ is taken here as a hard wall (but could also be an inflow or transparent boundary). At $x = L$ we take a hard wall boundary condition. Consider a wave that propagates to the right and arrives at $x = B$. This wave will continue to propagate to $x = L$, bounce back, and propagate to the left passing again the boundary at $x = B$.

**Problem** For instance $\eta(x,t)$ and $\phi(x,t)$ are the solutions on the physical domain $[0,L]$ with flat bathymetry and hard wall boundary conditions at $x=0$ and $x=L$. Take restriction of these solutions on $[0,B]$ as $(\eta_r,\phi_r)$.
Aim: Design EBC such that the problem on $[0,B]$ with EBC has solutions $(\eta_1,\phi_1)$ so that $\eta_1=\eta_r$ and $\phi_1=\phi_r$.

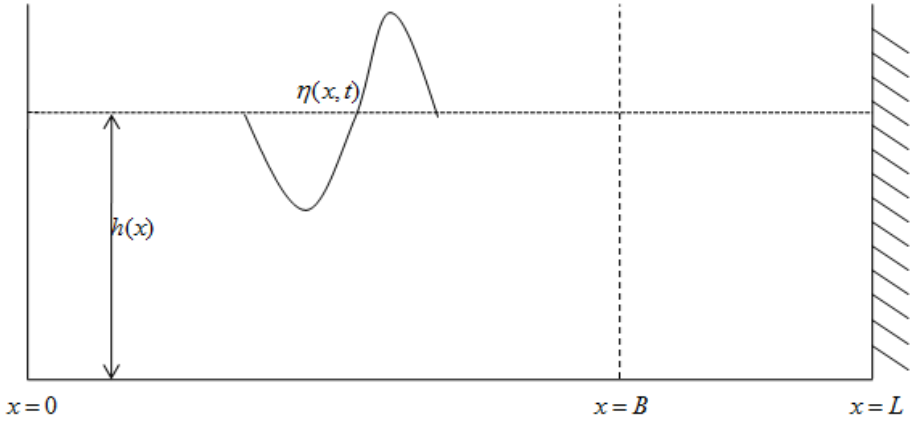


**Figure 3.1:** Effective boundary condition over flat bathymetry illustration

## 3.2 Effective Boundary Condition over Flat Bathymetry

For waves propagating over flat bottom ($h(x)=h$), linear SWE (2.14) in 1D have the general solutions:

$$\eta(x,t) = F_1(\frac{x}{c}-t) + G_1(\frac{x}{c}+t)$$
$$\phi(x,t) = F_2(\frac{x}{c}-t) + G_2(\frac{x}{c}+t),$$

in which $F_1$, $G_1$, $F_2$, and $G_2$ can be any function having two continuous derivatives with respect to $x$ and $t$.

For a right Influx Transparent Boundary Condition (ITBC), i.e. transparent for waves propagating to the right but influxing the waves propagating to the left, we assumed that the solution to the exterior of our computational domain is known. It is assumed that the solution outside the right BC is the propagating wave over a constant depth $h_R$ at the right boundary. So, the solutions to this type of wave are:

$$\eta(x,t) = F_1(\frac{x}{c_R} - t) + G_1(\frac{x}{c_R} + t)$$

$$\phi(x,t) = F_2(\frac{x}{c_R} - t) + G_2(\frac{x}{c_R} + t)$$

where $c_R = \sqrt{gh_R}$. Differentiation of $\phi(x,t)$ with respect to $x$ and $t$ at the neighbourhood of this point results in:

$$\partial_x \phi = \frac{1}{c_R} F_2^{'} + \frac{1}{c_R} G_2^{'}$$

$$\partial_t \phi = -F_2^{'} + G_2^{'}.$$

Elimination of $F_2^{'}$ yields the right ITBC as:

$$\partial_t \phi + c_R \partial_x \phi = 2G_2^{'}. \tag{3.1}$$

This is the condition for the right ITBC, where the influx signal at $x = x_R$ is given by $2G_2^{'}$.

Now, we can model the EBC over flat bathymetry as:

1. In order to measure the properties of the incoming wave $d(t)$ at $x = B$, we have the left ITBC (transparent for waves propagating to the left but influxing the waves propagating to the right):

$$\partial_t \phi - c_B \partial_x \phi = -2F'(\frac{x}{c_B} - t) \tag{3.2}$$

   where $c_B = \sqrt{gh_B}$, $h_B$ is the constant depth at $x = B$, and the influx signal at $x = B$ is given by $-2F'$, $F$ is the solution for the right wave potential velocity.

2. The theoretical model $M$ for this case is the time delay $2B/c_B$ needed by the waves to propagate back and forth on the domain $[B, L]$.

3. In the same way, the reflected wave $I$ at $x = B$ can be included with the right ITBC as:

$$\partial_t\phi + c_B\partial_x\phi = 2G'(\frac{x}{c_B} + t) \tag{3.3}$$

where the influx signal at $x = B$ is given by $2G'$, $G$ is the solution for the left wave potential velocity.

Since at $x = L$ the boundary is a hard wall, the waves that pass $x = B$ and bounce back at $x = L$, will pass $x = B$ with the same profile but in opposite direction, and with a time delay $2B/c_B$. Therefore, the EBC at $x = B$ will be:

$$(\partial_t\phi + c_B\partial_x\phi) \mid_t = (\partial_t\phi - c_B\partial_x\phi) \mid_{t-2B/c_B}, \tag{3.4}$$

with $\partial_t\phi - c_B\partial_x\phi = 0$ for $t < 2B/c_B$, with the assumption that the initial condition $\eta(x, 0) = 0$ and $\phi(x, 0) = 0$ on $[B, L]$, so there is no reflection wave yet for $t < 2B/c_B$. In the other words, the 'first' wave that enters $[B, L]$ will appear in the model after $2B/c_B$ $s$ time delay.

We can rewrite (3.4) by using (2.13b) as:

$$(\partial_t\phi + c_B\partial_x\phi) = -2g\eta - (\partial_t\phi + c_B\partial_x\phi).$$

Therefore the EBC at $x = B$ can be rewritten as:

$$(\partial_t\phi + c_B\partial_x\phi) \mid_t = -(2g\eta + (\partial_t\phi + c_B\partial_x\phi)) \mid_{t-2B/c_B} \tag{3.5}$$

with $2g\eta + (\partial_t\phi + c_B\partial_x\phi) = 0$ for $t < 2B/c_B$, which is easier and cheaper to be implemented in the numerical code than (3.4). This is because in (3.5) we can store the value of $\partial_t\phi + c_B\partial_x\phi$ for the whole iteration, instead of calculating the value of $\partial_t\phi - c_B\partial_x\phi$ in the right hand side of (3.4) every iteration.

## 3.3 Simulations

To validate the EBC that has been formulated, we will compare it with the computation in the whole domain $[0, L]$. For the simulation, the linear SWE code is used with

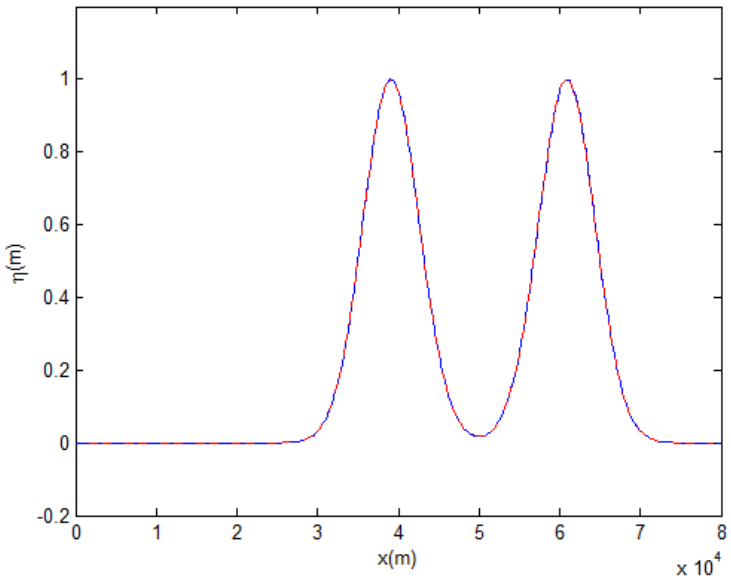


**Figure 3.2:** Comparison between the simulation on the whole domain (blue dashed line) and using EBC (red solid line) at $t = 15\,\text{min}$

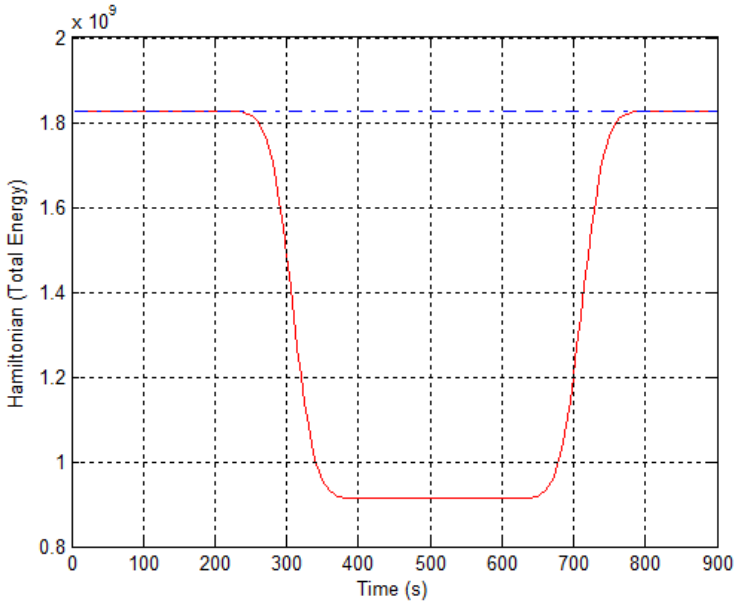


**Figure 3.3:** Comparison of the Hamiltonian between the simulation on the whole domain (blue dashed line) and using EBC (red solid line) for $t = 15\,\text{min}$

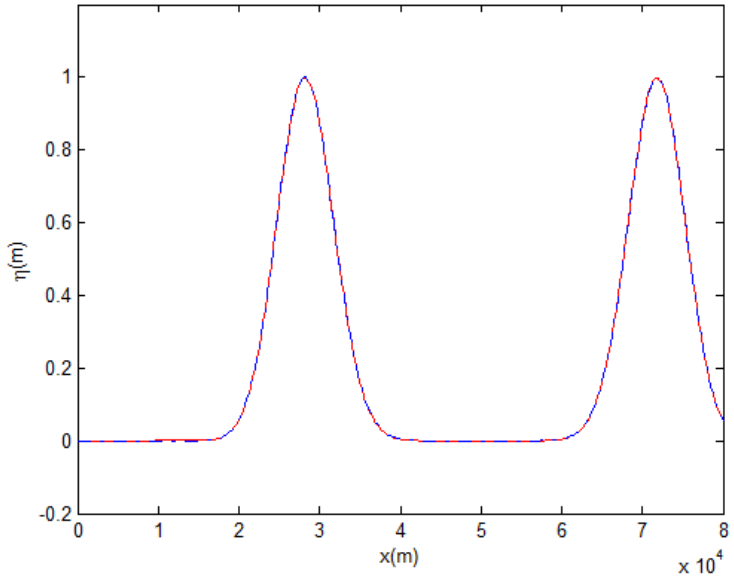


**Figure 3.4:** Comparison between the simulation on the whole domain (blue dashed line) and using EBC (red solid line) at $t = 30\,\text{min}$

$L = 100km$, $B = 80km$, $h = 1km$, $dx = 250m$, and $dt = 5s$. The simulation is uniform in $y$ direction, with $H = 15km$ and $dy = 1500m$.

The system of linear SWE (2.18) with EBC (3.5) is a type of *delay differential equation*, in which the derivative of the unknown function at a certain time $t$ is given in terms of the values of the function at previous times $t - 2B/c_B$. Problem of this type can be dealt with using *dde23* solver at MATLAB.

As initial condition we take a single hump in the middle of the whole domain with zero velocity everywhere, i.e.

$$\eta(x,0) = A \exp -(\frac{x - L/2}{50\sqrt{c}})^2$$

$$\phi(x,0) = 0$$

with $A = 2$. Because of the boundary conditions and the symmetric initial condition, the solutions is symmetric with respect to $x = L/2$ for all time.

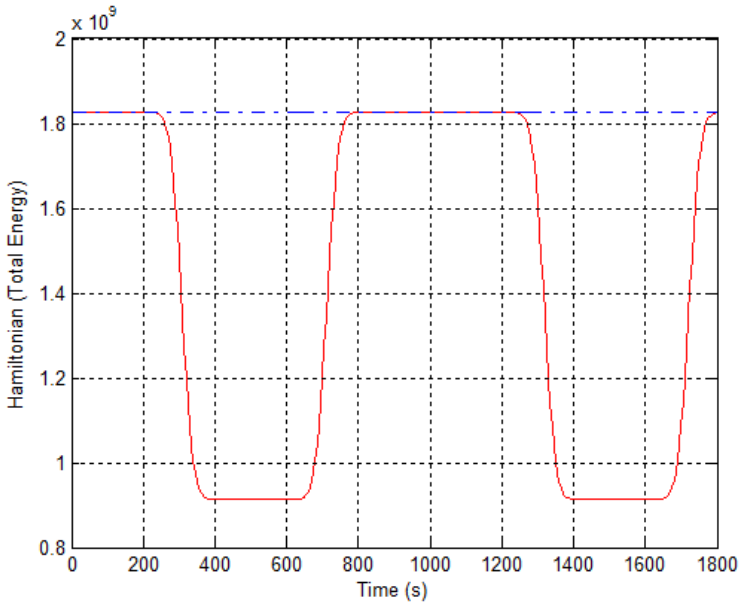


**Figure 3.5:** Comparison of the Hamiltonian between the simulation on the whole domain (blue dashed line) and using EBC (red solid line) for $t = 30\,\text{min}$

Fig. (3.2) and fig. (3.4) are comparisons of simulations with EBC and simulations on the whole domain. The blue dashed line represents the wave elevation calculated in the whole domain $[0, L]$, the red line represents the wave elevation using EBC at $x = B$. Fig. (3.2) is the comparison at $T = 15\,\text{min}$, when the waves have bounced once against the hard wall. Fig. (3.4) is the comparison at $T = 30\,\text{min}$, when the waves have bounced twice. Fig. (3.3) and fig. (3.5) are comparisons of the Hamiltonian (total energy) during the simulations; it is the integrated energy density over the whole interval $[0, L]$ or $[0, B]$, depending on the simulation case. We observe that the changing in the energy (once and twice) of the simulation with EBC, corresponds to the inflow and outflow of the waves in the calculation within the domain $[B, L]$.

**Numerical Performance.** For the first simulation, the CPU time for solving the PDE when calculated in the whole domain (using *ode45* solver) is $14s$, and when using EBC is $83s$. The increase of computational time when using EBC is because of the use of the solver *dde23* solver for the delay differential equation. In the second simulation, the CPU time for solving the PDE when calculated in the whole domain is

$27s$, and when using EBC is $187s$. Fig. (3.3) and fig. (3.5) are the comparisons of the Hamiltonian (total energy) during the simulations for the corresponding time. We can observe that there is some incoming and outgoing amount of energy on the simulation with EBC, which correspond to the waves calculated analytically within the domain $[B, L]$.

# 4

# Effective Boundary Condition over Slowly Varying Bathymetry

In this chapter, we will derive the Effective Boundary Condition (EBC) for waves propagating over a slowly varying bathymetry. In Section 4.1, we will start with WKB approximation, and continue with deriving the Reflection WKB approximation in Section 4.2. The challenges in deriving EBC (in Chapter 1) for this case will be answered. Challenges 1, 2, and 3 will be explained in Section 4.4, and challenge 4 in Section 4.5.

## 4.1 Problem Formulation

The physical domain from $x = 0$ until $x = L$ is divided into two parts, as shown in fig. (4.1). The domain $[0, B]$ will be calculated numerically, whereas the domain $[B, L]$ will be calculated analytically. In this chapter, the depth of the domain $h(x)$ will decrease slowly from $x = B$ until $x = L$, and with $h(x > L) = h(L)$. The boundary at $x = 0$ can be chosen as in Chapter 3. At $x = L$, the boundary is chosen to be transparent. For a wave that propagates to the right, passes the point $x = B$, will continue to $x = L$ and further.

**Problem** For instance $\eta(x, t)$ and $\phi(x, t)$ are the solutions on the physical domain $[0, L]$ with slowly varying bathymetry on $[B, L]$ and transparent boundary conditions at $x = 0$ and $x = L$. Take restriction of these solutions on $[0, B]$ as $(\eta_r, \phi_r)$.

Aim: Design EBC such that the problem on $[0, B]$ with EBC has solutions $(\eta_1, \phi_1)$ so that $\eta_1 = \eta_r$ and $\phi_1 = \phi_r$.

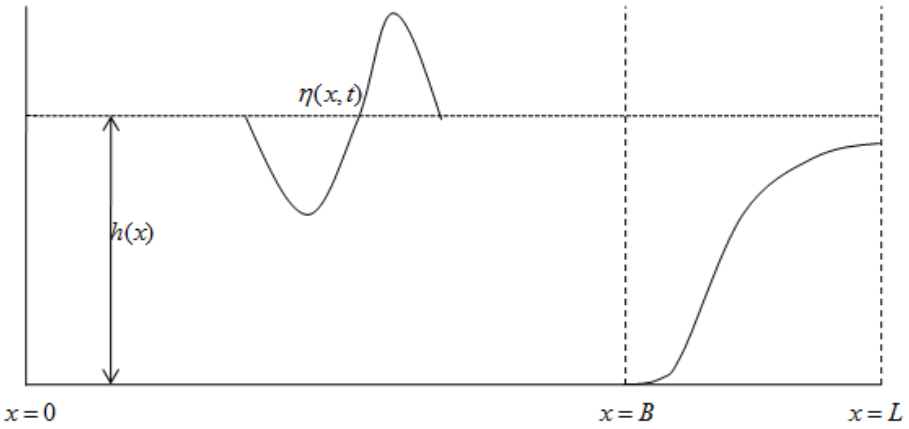


**Figure 4.1:** Effective boundary condition over slowly varying bathymetry illustration

## 4.2 WKB Approximation

For waves above a slowly varying bathymetry, there is a very good approximation termed the Wentzel-Kramer-Brillouin (WKB) approximation (van Groesen and Molenaar 2007, Hinch 1991). The variations in the water depth are slow if $\Delta h/\overline{L} << 1$, where $\Delta h$ is the change in depth over a horizontal distance $\overline{L}$ (fig. 4.2). By rewriting again eq. (2.14) in one dimension, we get:

$$\partial_t^2 \eta - \partial_x \left[ c^2 \partial_x \eta \right] = 0. \tag{4.1}$$

The differential equation (4.1) can be solved easily for constant $c$. Only for some special functions $c = c(x)$, one can solve this differential equation analytically.

Following van Groesen and Molenaar, for a slowly varying velocity $c(\epsilon x)$, we take as Anzats for (4.1):

$$\eta\left(x,t\right) = \rho\left(\epsilon x\right) F\left(\theta\left(x,t\right)\right) \tag{4.2}$$

where the profile function $F$ is arbitrary, the phase $\theta$ satisfies the eiconal equation:

$$\left(\partial_t \theta\right)^2 = c^2 \left(\partial_x \theta\right)^2 \tag{4.3}$$

and the amplitude $\rho$ satisfies

$$\rho(\epsilon x) = \frac{A}{\sqrt{c(\epsilon x)}}. \tag{4.4}$$

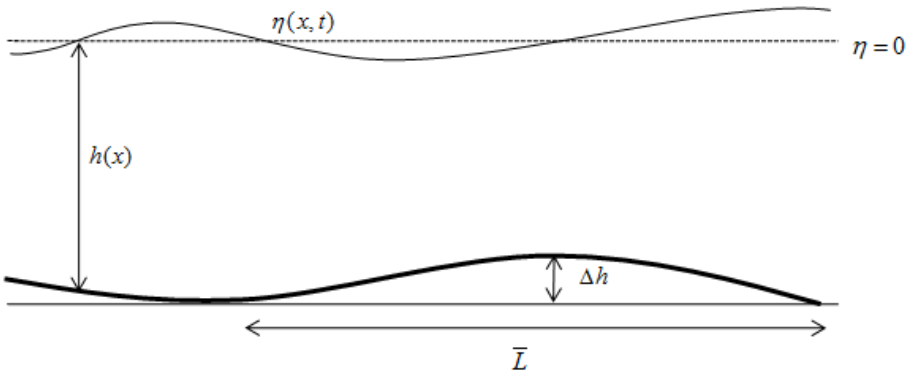


**Figure 4.2:** Slowly varying bathymetry

This solution can be obtained by substituting (4.2) to (4.1). By regrouping the terms, we will get

$$\partial_t^2 \eta - \partial_x c^2(\epsilon x)\,\partial_x \eta = r_0 F'' + r_1 F' + r_2 F \tag{4.5}$$

with $r_0 = \rho\theta_t^2 - \rho c^2 \theta_x^2$, $r_1 = \rho\theta_{tt} - 2\epsilon c^2 \rho_x \theta_x - 2\epsilon c c_x \rho \theta_x - c^2 \rho \theta_{xx}$, and $r_2 = \epsilon^2 \partial_x \left(c^2 \partial_x \rho\right)$. Requiring $r_0 = 0$ will lead to (4.3). Then $r_1 = 2\epsilon c \rho_x + \epsilon \rho c_x$, and requiring this to vanish leads to (4.4). Since both $c$ and $\rho$ are slowly varying, the order of the remaining residue $r_2$ is then $\mathcal{O}\left(\epsilon^2\right)$ as in the WKB approximation.

Thus, the WKB approximation for right traveling waves is

$$\eta(x,t) = \frac{A}{\sqrt{c(x)}} F\left(t - \int_0^x \frac{1}{c(\zeta)} d\zeta\right). \tag{4.6}$$

It can be observed that this is precisely the solution of

$$\partial_t \eta + \sqrt{c}\partial_x \sqrt{c}\eta = 0, \tag{4.7}$$

which can be checked by subsituting (4.6) to (4.7).

## 4.3 Reflection WKB Approximation

Because our aim is to look for the expression of reflected waves that travels to the left for right travelling waves, we will write the total wave elevation ($\eta$) as the sum of a right ($\overrightarrow{\eta}$) and a left (reflected) wave $\left(\overleftarrow{\xi}\right)$, i.e.

$$\eta = \overrightarrow{\eta} + \overleftarrow{\xi}. \tag{4.8}$$

Anticipating the WKB-equation for right and left travelling waves, we observe that

$$(\partial_t + \sqrt{c}\partial_x\sqrt{c})(\partial_t - \sqrt{c}\partial_x\sqrt{c}) = \partial_t^2 - \sqrt{c}\partial_x c\partial_x\sqrt{c}.$$

Hence, we rewrite equation (4.1) as

$$\left(\partial_t^2 - \sqrt{c}\partial_x c\partial_x\sqrt{c} - \left(\partial_x c^2\partial_x - \sqrt{c}\partial_x c\partial_x\sqrt{c}\right)\right)\eta = \left(\partial_t^2 - \mathcal{D}^2 - b\right)\eta = 0,$$

where we use the operator $\mathcal{D}(.) = \sqrt{c}(\partial_x\sqrt{c}(.))$, and define $b(.) = \partial_x(c^2\partial_x(.)) - \sqrt{c}\partial_x(c\partial_x(\sqrt{c}(.)))$.

With (4.8) we get

$$\left(\partial_t^2 - \mathcal{D}^2\right)\overrightarrow{\eta} + \left(\partial_t^2 - \mathcal{D}^2\right)\overleftarrow{\xi} = b\overrightarrow{\eta} + b\overleftarrow{\xi}. \tag{4.9}$$

The first term in the left hand side vanishes by (4.7). The first term in the right hand side is a simple multiplication operator $b\overrightarrow{\eta} = -\frac{1}{4}\epsilon^2(c'(x)^2 + 2c(x)c''(x))\overrightarrow{\eta}$, which is the WKB approximation's residue of $\mathcal{O}\left(\epsilon^2\right)$. The second term $b\overleftarrow{\xi}$ will be of higher order and will be neglected in the following. The remaining terms are

$$\left(\partial_t + \mathcal{D}\right)\left(\partial_t - \mathcal{D}\right)\overleftarrow{\xi} = b(x)\overrightarrow{\eta}. \tag{4.10}$$

For simplicity, we will use $\eta$ for $\overrightarrow{\eta}$ and $\xi$ for $\overleftarrow{\xi}$ in the rest of this section. To solve (4.10), we will do some algebraic steps and a transformation such that we can get the analytical solution for the reflection wave in a simpler form. By defining $\left(\partial_t - \mathcal{D}\right)\xi = \lambda$, we can rewrite (4.7) and (4.10) as a system of differential equations

$$\begin{gathered}\left(\partial_t + \mathcal{D}\right)\eta = 0 \\ \left(\partial_t + \mathcal{D}\right)\lambda = b(x)\eta \\ \left(\partial_t - \mathcal{D}\right)\xi = \lambda.\end{gathered}$$

By multiplying all the equations with $\sqrt{c(x)}$, the system become

$$\begin{gathered}(\partial_t + c\partial_x)\,\overline{\eta} = 0 \\ (\partial_t + c\partial_x)\,\overline{\lambda} = b(x)\overline{\eta} \\ (\partial_t - c\partial_x)\,\overline{\xi} = \overline{\lambda}.\end{gathered}$$

for $\overline{\eta} = \sqrt{c}\eta$, $\overline{\lambda} = \sqrt{c}\lambda$, and $\overline{\xi} = \sqrt{c}\xi$.

After introducing the time independent variable

$$y = y(x) \text{ such that } \partial_y = c\partial_x \rightarrow y = \int_0^x \frac{d\zeta}{c(\zeta)}$$

our system becomes a system with constant coefficients

$$(\partial_t + \partial_y)\,\overline{\eta} = 0 \tag{4.11}$$

$$(\partial_t + \partial_y)\,\overline{\lambda} = b(y)\overline{\eta} \tag{4.12}$$

$$(\partial_t - \partial_y)\,\overline{\xi} = \overline{\lambda}. \tag{4.13}$$

The solution of this system can be found successively:

(i) Given the initial condition $\eta(x,0) = F(x)$ then $\overline{\eta}\,(x,0) = \sqrt{c(x)}F(x) = \bar{F}(x)$, and the first equation has the solution

$$\overline{\eta} = \bar{F}(y-t) \tag{4.14}$$

which is actually the WKB solution (4.6).

(ii) Since we have $(\partial_t - \mathcal{D})\,\xi = \lambda$ and $\xi(x,0) = 0$, it follows that $\lambda(x,0) = 0$. By substituting (4.14) to (4.12), the general solution $\overline{\lambda}$ is given by

$$\overline{\lambda} = \bar{F}(y-t)\,\mathcal{B}(y) + G_1(y-t) \text{ with } \mathcal{B}(y) = \int_0^y b(\zeta)d\zeta,$$

and $G_1$ can be any function. $\mathcal{B}(y)$ is only nonvanishing for $x > B$ so $G_1(y-t) = 0$ and the particular solution for $\overline{\lambda}$ is

$$\overline{\lambda} = \bar{F}(y-t)\,\mathcal{B}(y) \text{ with } \mathcal{B}(y) = \int_0^y b(\zeta)d\zeta. \tag{4.15}$$

(iii) By substituting (4.15) to (4.13), we obtain the general solution of $\overline{\xi}$ as

$$\overline{\xi} = -\int_0^y \bar{F}(2\beta - (y+t))\mathcal{B}(\beta)\, d\beta + G_2(y+t),$$

with $G_2$ can be any function. At $t = 0$, we have no reflection wave, $\xi(x, 0) = 0$, so the particular solution for $\overline{\xi}$ is

$$\begin{aligned}\overline{\xi} &= -\int_0^y \bar{F}(2\beta - (y+t))\mathcal{B}(\beta)\, d\beta + \int_0^{y+t} \bar{F}(2\beta - (y+t))\mathcal{B}(\beta)\, d\beta \\ &= \int_y^{y+t} \bar{F}(2\beta - (y+t))\mathcal{B}(\beta)\, d\beta \end{aligned} \tag{4.16}$$

**Comparison between Reflection WKB approximation and numerical solutions.** Before continuing with the EBC over slowly varying bathymetry, we will compare this analytical solution of Reflection WKB approximation with numerical solutions. We will perform the simulation on the domain $[-100, 100]km$ with the same parameters used in the previous chapter, for total simulation time $t = 25min$. The bathymetry is defined by

$$h(x) = -\frac{h_0 - h_1}{2}\ \tanh((x-m)/w) + \frac{h_0 + h_1}{2},$$

where $h_0 = 1000m$ is the depth before the slowly varying bathymetry and $h_1 = 100m$ is the depth after the slowly varying bathymetry, $m$ is the 'middle' of the slope and $w$ is the 'half width' of the slope.

In the 3 cases to follow we take $m = 50km$ and 3 different slopes of the bottom by taking $w = 5km$ (slope 1:15), $w = 10km$ (slope 1:30), and $w = 15km$ (slope 1:45). We present the results of the waves: with blue dashed line is the numerical solution and with red solid line is the analytical solution. Figure (4.3) is the comparison between the numerical and analytical solution for slope 1:15. From this simulation, it can be seen that the numerical solution has a small negative wave approximately at $x = 80km$. And by looking at the analytical solution (the red solid line), actually this is the reflected waves that going to the left. A big part of reflection waves will propagate to the right, but a small part of it will propagate to the right. This also explains eq. (4.10), where $\overleftarrow{\xi}$ actually satisfies 'total' wave equation (which already neglects the $b\overleftarrow{\xi}$ term).

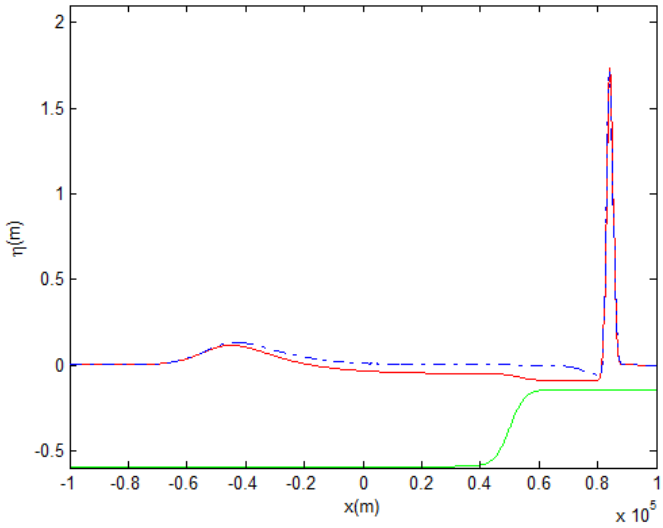


**Figure 4.3:** Comparison of numerical (blue dashed line) and analytical (red solid line) solution for steep slope ($w = 5km$)

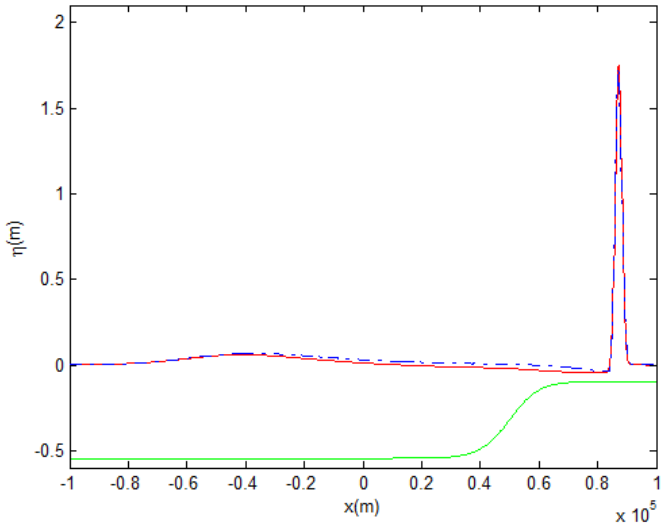


**Figure 4.4:** Comparison of numerical (blue dashed line) and analytical (red solid line) solution for mild slope ($w = 10km$)

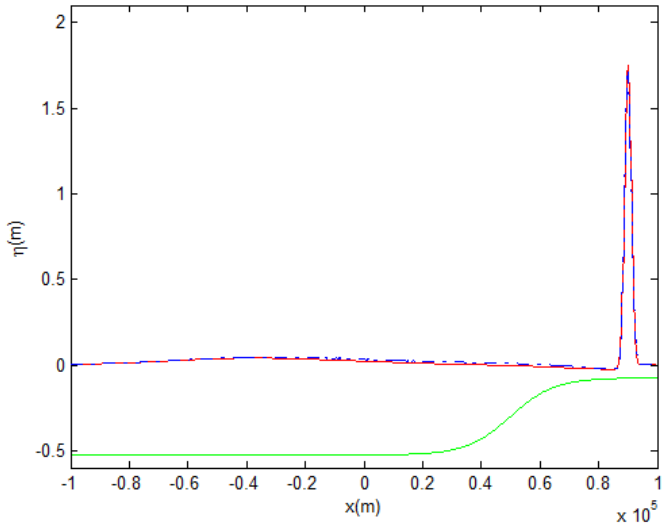


**Figure 4.5:** Comparison of numerical (blue dashed line) and analytical (red solid line) solution for very mild slope ($w = 15km$)

The quite large error between the numerical and the analytical solution may be caused by the fact that the bathymetry varies not slowly enough, since the analytical solution actually only valid in slowly varying bathymetry. Therefore, comparisons were done for milder slopes 1:30 in fig (4.4) and 1:45 in fig (4.5). These comparisons show that the analytical solutions get closer and closer to the numerical one.

Fig. (4.6) shows the plot of $\overrightarrow{\eta}(x,t)$, $\overleftarrow{\xi}(x,t)$, and $\lambda(x,t)$ at $t = 25min$ for the case $w = 10km$. The plot of $b(x)$ and $\mathcal{B}(x)$ can be seen in fig. (4.7) and fig. (4.8). It can be observed that $\mathcal{B}(x)$ is nonvanishing on the slope, and this generates $\lambda(x,t)$ (see eq. (4.15)) after the propagating waves $\overrightarrow{\eta}(x,t)$ enter the slope, and at last will generate the reflection waves $\overleftarrow{\xi}(x,t)$.

The comparison of the WKB approximation ($\overrightarrow{\eta}(x,t)$), the Reflection WKB approximation ($\overrightarrow{\eta}(x,t) + \overleftarrow{\xi}(x,t)$), and the numerical solution for the case $w = 5km$ ($dx = 125m$) is shown in fig. (4.9). Here we can see more clearly (also from fig. (4.6)) that the WKB approximation for $\overrightarrow{\eta}(x,t)$ only will not give the small negative waves for the left propagating waves over the slowly varying bathymetry. The Reflection WKB approximation also gives better approximation for the maximum waveheight

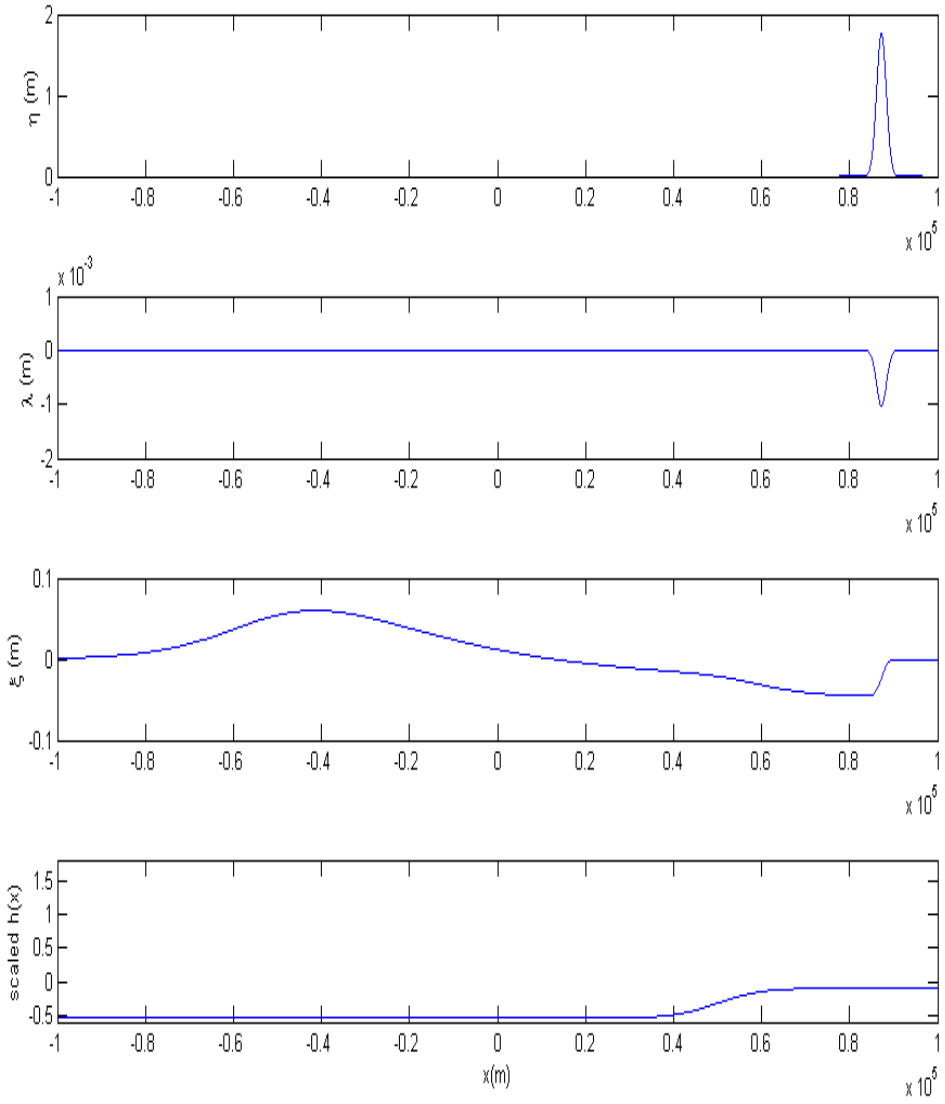


**Figure 4.6:** Plot of $\overrightarrow{\eta}(x,t)$, $\lambda(x,t)$, $\overleftarrow{\xi}(x,t)$, and $h(x)$

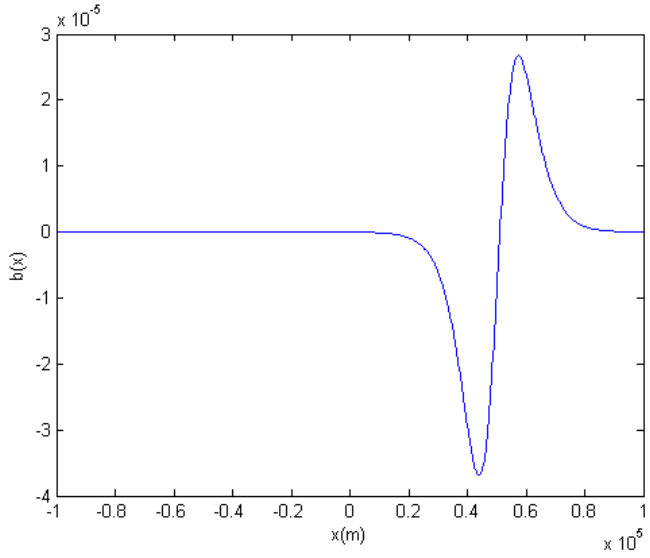


**Figure 4.7:** Plot of $b(x)$

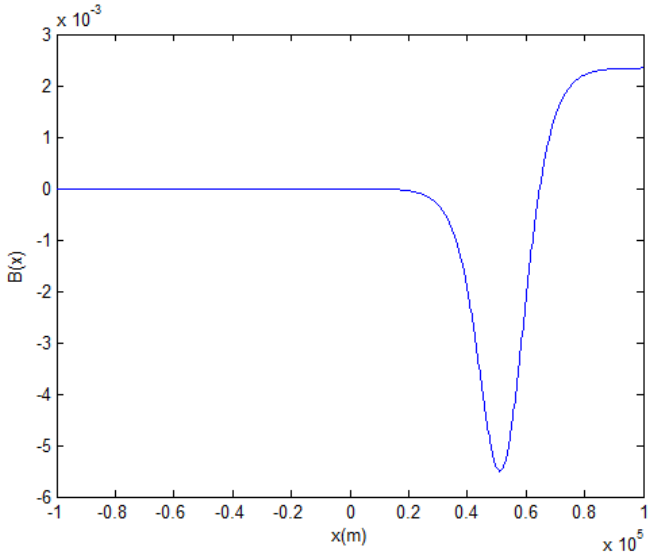


**Figure 4.8:** Plot of $\mathcal{B}(x)$

compared to the numerical solution. Therefore, we can claim that this Reflection WKB approximation corrects the WKB approximation for the left propagating waves.

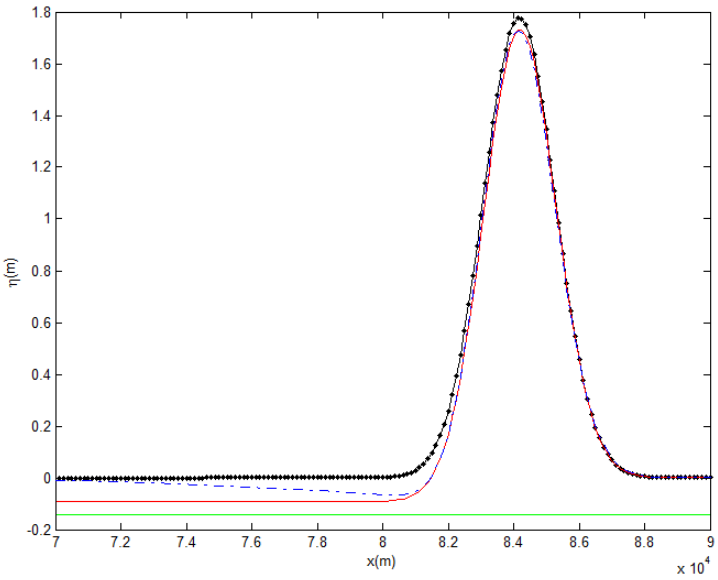


**Figure 4.9:** Comparison between the WKB approximation (black dotted line), the Reflection WKB approximation (red solid line), and the numerical solution (blue dashed line)

## 4.4 Effective Boundary Condition over Slowly Varying Bathymetry

1. Given the solution for the right propagating waves $\eta(x,t) = F(\frac{x}{c} - t)$, the properties of the incoming wave $d(t)$ at $x = B$ is given by

$$\eta(x,t)|_{x=B} = F(\frac{B}{c_B} - t), \tag{4.17}$$

with $c_B = \sqrt{gh_B}$, $h_B$ is the constant depth before the slope ($x < B$).

2. The theoretical model for the shore $M(d)$ is given by the Reflection WKB approximation in $y$ variable as:

$$\overline{\xi}(y,t) = \int_y^{y+t} \bar{F}(2\beta - (y+t))\mathcal{B}(\beta)\, d\beta \tag{4.18}$$

3. The reflected wave $I$ at $x = B$ can be included with the right ITBC as:

$$\partial_t\phi + c_B\partial_x\phi = 2G'(\frac{x}{c_B} + t) \tag{4.19}$$

where the influx signal at $x = B$ is given by $2G'$, $G$ is the solution for the left wave potential velocity (as derived in Section 3.2).
Thus, with the relation $\partial_t\phi = -g\eta$, the EBC over slowly varying bathymetry can be formulated as:

$$\partial_t\phi + c_B\partial_x\phi = -2g\overleftarrow{\xi}(B,t), \tag{4.20}$$

with $\overleftarrow{\xi}(x,t)$ is given by (4.18) after transforming back to $x$ variable.

## 4.5 Simulations

For checking the EBC implementation, we will compare it with the numerical solution on the whole domain. For the EBC simulation, we will use the domain $[-100, 20]km$ and the other parameters are the same as in the previous subsection. Fig (4.10)-(4.12) shows the comparison of reflection waves between the simulation on the whole domain and with EBC in part of the domain for $w = 5km$ (slope 1:15), $w = 10km$ (slope 1:30), and $w = 15km$ (slope 1:45). The blue dashed line represents the reflection wave calculated in the whole domain $[-100, 100]km$, the red one represents the reflection wave using EBC at $x = 20km$. Here it can be seen clearly that there is quite large error between the numerical and the analytical solution that may be caused by the fact that the bathymetry varies not slowly enough, since the analytical solution actually only valid in slowly varying bathymetry. It can be seen that when the slope is steeper, the error is larger.

**Numerical Performance.** For the case $w = 10km$, the CPU time for solving the PDE when calculated in the whole domain is $86s$. The CPU time needed to calculate the reflection wave analytically is $4.56s$ and the CPU time to solve the PDE in part of the domain, together with influxing the EBC is $69s$. This numerical performance shows that the use of EBC can reduce the computational time.

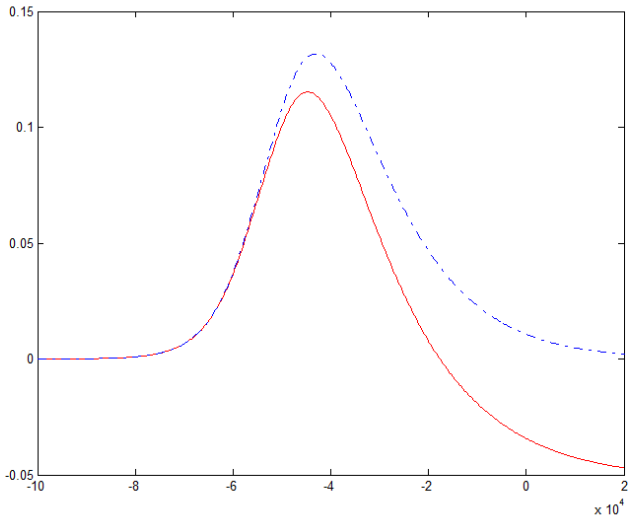


**Figure 4.10:** Comparison between the simulation on the whole domain (blue dashed line) and using EBC (red solid line) for steep slope ($w = 5km$)

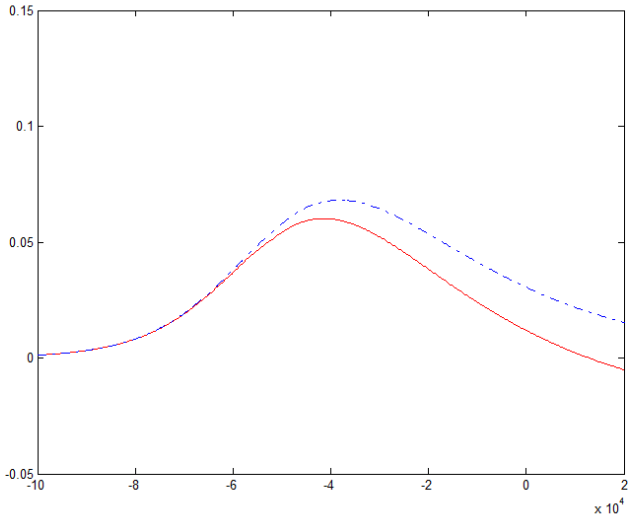


**Figure 4.11:** Comparison between the simulation on the whole domain (blue dashed line) and using EBC (red solid line) for mild slope ($w = 10km$)

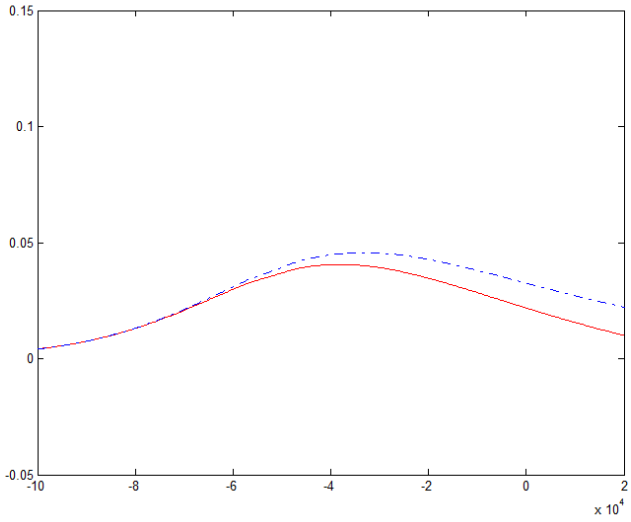


**Figure 4.12:** Comparison between the simulation on the whole domain (blue dashed line) and using EBC (red solid line) for very mild slope ($w = 15km$)

# 5

# Conclusions and Future Work

## 5.1 Conclusions

The effective boundary conditions (EBCs) is designed with the aim to calculate more accurate wave interactions near the shore without increasing the computational cost. In this thesis, the EBCs over flat bathymetry and over slowly varying bathymetry have been derived. Both of these EBCs have been implemented and compared with the numerical solution where the calculation on the shore was also included.

For the EBC over flat bathymetry, the comparison between the EBC calculation and the numerical solution on the whole domain shows good agreements. One of the results can be seen in fig. (3.4). We found that the computational time using the EBC is more expensive because of the use of the *dde*23 solver for time integration in MATLAB to solve the delay differential equation. This problem may can be overcome by developing our own code with fix time discretization to solve the time integration, since MATLAB uses its own time discretization.

The comparison between the EBC calculation over slowly varying bathymetry and the numerical solution on the whole domain shows that there is quite some error; this is expected because of the second order WKB approximation. One of the result can bee seen in fig. (4.11). The results show that when the slope is steeper, the error is larger. This problem may can be overcome by deriving the higher order WKB approximation or doing iteration in calculating $\overleftarrow{\xi}$ such that the second term in the right hand side of

equation (4.9), which is neglected in this thesis, can be included in the calculation.

As an additional result, the Reflection WKB approximation has been derived in this thesis, which not only models the reflected wave, but also improves the WKB approximation for the wave that propagates over the slowly varying bathymetry. The comparison for the WKB approximation, the Reflection WKB approximation, and the numerical solution is shown in fig. (4.9)

## 5.2 Future Work

For future work, the EBC when there is run-up and run-down on the shore will be interesting. The model of wave propagation in the sea, which is kept simple as the linear SWE model in this report can also be improved to a more accurate model, e.g. linear VBM and models which include nonlinearity.

# Appendix A

# Numerical Solution of linear Shallow Water Equations and linear Variational Boussinesq Model

## A.1 Two Dimensional Finite Element Method: Quadrilateral Element

We will use quadrilateral elements for approximating the solution of linear SWE, and we will start with the simple case of a rectangle with all sides in the coordinates directions. Such a rectangle may be considered as the product of two one-dimensional elements in $x$ and $y$- direction respectively. The simplest element is the one with the 4 vertices as nodes and a bilinear approximation.

The basis function for a rectangle as illustrated at fig.(A.1). can be defined by:

$$T_1(x, y) = \lambda_1(x)\lambda_1(y)$$

$$T_2(x, y) = \lambda_2(x)\lambda_1(y)$$

$$T_3(x, y) = \lambda_2(x)\lambda_2(y)$$

# A. NUMERICAL SOLUTION OF LINEAR SHALLOW WATER EQUATIONS AND LINEAR VARIATIONAL BOUSSINESQ MODEL

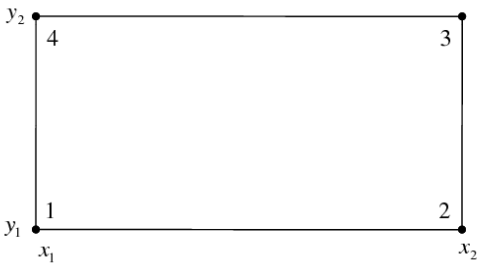


**Figure A.1:** Quadrilateral element

$$T_4(x,y) = \lambda_1(x)\lambda_2(y) \tag{A.1}$$

with $\lambda_i(x)$ is one-dimensional basis functions in $x$-direction and $\lambda_j(y)$ in $y$-direction. We can verify that the basis function $T_i(x,y)$ in (A.1) have the shape

$$T_i(x,y) = a_0^i + a_1^i x + a_2^i y + a_3^i xy. \tag{A.2}$$

But unfortunately the basis functions of the shape (A.2) are not continuous for a general quadrilateral. Since it is not clear what the general shape of the basis functions must be, we have to use some special construction method. The standard technique is known as *isoparametric transformations*. The idea is we do not know what the basis functions look like for a general quadrilateral, but for a square with sides in $x$ and $y$-direction is obvious. So, we can transform the general quadrilateral element in the $x-y-$plane with a coordinate transformation $(x,y) \rightarrow (\xi,\eta)$ to a *standard element* (the unit square) in the $\xi-\eta-$plane. Such a transformation is called isoparametric if it is satisfies the following properties:

1. The nodes $\mathbf{x}_1, \mathbf{x}_2, ..., \mathbf{x}_k$ are transformed to fixed point $\xi_1, \xi_2, ..., \xi_k$, i.e. the points in the reference element are always the same.

2. Straight sides in the original element remain straight in the reference element.

3. If the basis functions in the transformed element are given by $T_1(\mathbf{x}), T_2(\mathbf{x}), ...T_k(\mathbf{x})$

then the inverse transformation $(\xi, \eta) \to (x, y)$ is given by

$$\mathbf{x} = \sum_{l=1}^{k} \mathbf{x}_l T_l(\xi, \eta) \tag{A.3}$$

and the interpolation by

$$u(\mathbf{x}) = \sum_{l=1}^{k} u_l T_l(\xi, \eta) \tag{A.4}$$

In the other words, we use the same element for transformation and interpolation.

We will do the *bilinear transformation*. The nodes $\mathbf{x}_i$ of the quadrilateral are transformed to the vertices of the unit square in the following way:

$$\mathbf{x}_1 \to (0,0)\,,\ \mathbf{x}_2 \to (1,0)\,,\ \mathbf{x}_3 \to (1,1)\,,\ \mathbf{x}_4 \to (0,1) \tag{A.5}$$

The basis functions in the $(\xi, \eta)$-plane are bi-linier and defined by

$$T_1 = (1-\xi)(1-\eta)\,,\ T_2 = \xi(1-\eta)\,,\ T_3 = \xi\eta,\ T_4 = (1-\xi)\eta \tag{A.6}$$

In order that the transformation is applicable, it must be invertible, i.e. for each $\mathbf{x}$ in the quadrilateral, there must be a unique $\xi$. So the Jacobian of the transformation must be non-singular for each $\mathbf{x}$ in the quadrilateral. The Jacobian matrix $\mathbf{J}$ is defined by:

$$\mathbf{J} = \begin{bmatrix} \frac{\partial x}{\partial \xi} & \frac{\partial x}{\partial \eta} \\ \frac{\partial y}{\partial \xi} & \frac{\partial y}{\partial \eta} \end{bmatrix} \tag{A.7}$$

and by transformation (A.3), the determinant of $J$ is given by:

$$\det(\mathbf{J}) = (x_2 - x_1 + A_x\eta)(y_4 - y_1 + A_y\xi) - (x_4 - x_1 + A_x\xi)(y_2 - y_1 + A_y\eta), \tag{A.8}$$

with $A_x = x_1 - x_2 + x_3 - x_4$ and $A_y = y_1 - y_2 + y_3 - y_4$.

By Newton Cotes rule, then the integration of the reference element (A.5) is given by the two-dimensional equivalent of the Trapezoid rule:

$$\int_0^1 \int_0^1 Int(\xi,\eta)d\xi d\eta \approx \frac{1}{4}\sum_{k=1}^{4} Int(\xi_k,\eta_k) \tag{A.9}$$

## A.2 FEM Implementation for linear SWE

By using the Newton Cotes rule (A.9), then the approximation of $m_{ij}$ and $g_{ij}$ in (2.18) will be

$$m_{ij} \approx \frac{1}{4}\sum_{k=1}^{4} \left(T_i T_j \left|J\right|\right)(\xi_k,\eta_k) \text{ and } g_{ij} \approx \frac{1}{4}\sum_{k=1}^{4} (h\nabla T_i \cdot \nabla T_j \left|J\right|)(\xi_k,\eta_k) \tag{A.10}$$

The values of $|J|$ in the integration points in the reference element can be computed immediately from eq. (A.8). To compute the values of $\nabla T_i$ we have to express the derivatives to $x$ and $y$ into derivatives of $\xi$ and $\eta$, since $T_i$ is only known in the $(\xi,\eta)$-plane:

$$\frac{\partial T_k}{\partial x} = \frac{\partial T_k}{\partial \xi}\frac{\partial \xi}{\partial x} + \frac{\partial T_k}{\partial \eta}\frac{\partial \eta}{\partial x},$$

$$\frac{\partial T_k}{\partial y} = \frac{\partial T_k}{\partial \xi}\frac{\partial \xi}{\partial y} + \frac{\partial T_k}{\partial \eta}\frac{\partial \eta}{\partial y}.$$

To compute these derivatives, we need the values of $\frac{\partial \xi}{\partial x}$ and so on, that can be calculated as the inverse of the Jacobian matrix $\mathbf{J}$.

### A.2.1 FEM Implementation for Boundary Conditions

To implement linear SWE as wave models for tsunami simulation, we need boundary conditions. At this moment, we will use two types of boundary conditions, i.e. hardwall boundary condition (HBC) and influx transparent boundary condition (ITBC).

### A.2.1.1 Hard wall Boundary Condition

In the HBC, the normal flow through the boundary is assumed to be zero or $\mathbf{U}.\mathbf{n} = 0$, where $\mathbf{U}$ is fluid velocity. Note that we approximate the velocity potential at each depth by its value at the surface: $\Phi(\mathbf{x}, z, t) \approx \phi(\mathbf{x}, t)$, so the condition for hardwall can be rewritten as $\nabla\phi.\mathbf{n} = 0$ (since $U = \nabla_3\Phi$ and $\Phi \approx \phi$). The derivation of the governing equations of linear SWE from the first variation (2.12a)-(2.12b) do not give the corresponding boundary condition because the functional that we minimized accounts only for the interior (from Pressure principle in (2.1)). We need to modify the weak formulation in order to incorporate the boundary conditions. Therefore, we use the corresponding governing equations from the weak formulation of (2.13a)-(2.13b) only for implementing the BC. To have the weak formulation of (2.13a)-(2.13b), we multiply the first equation of (2.13a)-(2.13b) by a test function and integrate it over a domain, then we do partial integration for the right hand side term, so we obtain the following equation for linear SWE

$$\int_\Omega v\partial_t\eta d\mathbf{x} = \int_\Omega h(\mathbf{x})\nabla\phi.\nabla v d\mathbf{x} - \int_{\partial\Omega} \left(vh\left(\mathbf{x}\right)\nabla\phi.\mathbf{n}\right) d\partial\Omega \tag{A.11}$$

For HBC, the condition $\nabla\phi.\mathbf{n} = 0$ has to be satisfied in the boundary term(s) of (A.11). This condition makes the boundary term in (A.11) vanishes. With this condition, we will have the system of matrix equation exactly the same with our system in (2.18). So the HBC's FEM implementation for SWE gives the same system of matrix equation as we derived based on the variational principle, where the BC term is ignored.

### A.2.1.2 Periodic Boundary Condition

The Periodic Boundary Condition (PBC) in 2 dimensional case are

$$\eta(0, y, t) = \eta(L, y, t) \text{ and } \eta(x, 0, t) = \eta(H, 0, t) \tag{A.12a}$$

$$\phi(0, y, t) = \phi(L, y, t) \text{ and } \phi(x, 0, t) = \phi(H, 0, t) \tag{A.12b}$$

with $L$ is the length of the domain in $x-$direction and $H$ is the length of the domain in $y$-direction.

#### A.2.1.3 Influx Transparent Boundary Condition

In the same way with deriving the Influx Transparent Boundary Condition (ITBC) for 1D case Section 3.2, thus for 2D case the right ITBC will be

$$\partial_t \phi + c\nabla\phi \cdot \mathbf{n} = 2G_2^{'}. \tag{A.13}$$

where $\mathbf{n}$ is outward normal direction at the boundary, $G_2$ is the solution for the left wave potential velocity.

Including the right ITBC (A.13) into the last term in the RHS of (A.11) gives

$$\int_\Omega v\partial_t \eta d\mathbf{x} = \int_\Omega h(\mathbf{x})\nabla\phi.\nabla v d\mathbf{x} - \int_{\partial\Omega} \left( vh\left(\mathbf{x}\right)\left( -\frac{1}{c}\partial_t\phi + \frac{2}{c}G_2^{'}\right)\right) d\partial\Omega \tag{A.14}$$

From (2.13b) we have the relation $\partial_t\phi = -g\eta$, so (A.14) is equivalent with

$$\int_\Omega v\partial_t \eta d\mathbf{x} = \int_\Omega h(\mathbf{x})\nabla\phi.\nabla v d\mathbf{x} - \int_{\partial\Omega} \left( v\left(c\eta - 2cG_1\right)\right) d\partial\Omega, \tag{A.15}$$

with $G_1$ is the solution for the left wave elevation.

For FEM implementation for the linear SWE with ITBC, we will use this last equation instead of (2.11a), by setting that test function $v = \delta\phi$. Now we will only treat the boundary term, because the rest is the same with (2.18). The boundaries in a 2D domain are basically a curve, so the boundary integration in (A.15) is implemented as if in 1D FEM. In 1D case, we use a linear basis function which is given by

$$T1_k(x) = \begin{cases} \left(\frac{x-x_{k-1}}{x_k - x_{k-1}}\right), x \in [x_{k-1}, x_k] \\ \left(\frac{x-x_{k+1}}{x_k - x_{k+1}}\right), x \in [x_k, x_{k+1}] \\ 0, \text{ elsewhere} \end{cases} \tag{A.16}$$

We approximate $v$, , $\eta$, and $G_1$ in boundary term of (A.15) by linear combination of basis function in 1D (A.16), then substitute these approximations into the boundary term. This will gives a matrix called $\mathbf{B}$ which is assembled from a $2 \times 2$ elementary matrix, in which the entries are given by

$$b_{ij} = \sqrt{g}\int_{\partial\Omega} \sqrt{h(x)} T1_i(x) T1_j(x) d\partial\Omega, \text{ with } i,j = 1,2$$

then approximation $\sqrt{h(x)} = \sum_{i=1}^{n} \sqrt{\hat{h_i}} T1_i(x)$, gives

$$B_{e_k} = \sqrt{g}\Delta_k \begin{pmatrix} \frac{\sqrt{h_1}}{4} + \frac{\sqrt{h_2}}{12} & \frac{\sqrt{h_1}+\sqrt{h_2}}{12} \\ \frac{\sqrt{h_1}+\sqrt{h_2}}{12} & \frac{\sqrt{h_1}}{12} + \frac{\sqrt{h_2}}{4} \end{pmatrix}$$

where $e_k$ denotes the $k$-th element in the boundary, $\Delta_k$ is the length between two points of the element in the boundary, and $h_1$ and $h_2$ are the depth in the points of element at the boundary (the indices correspond to the local numbering, note that the local numbering for 1D case are 1 and 2). With the presence of the boundary term, our system of matrix equation (2.18) will be

$$\mathbf{M}\partial_t \overrightarrow{\eta} = \mathbf{G}\overrightarrow{\phi} - \mathbf{B}\overrightarrow{\eta} + \mathbf{B}\overrightarrow{G_1}$$

$$\mathbf{M}\partial_t \overrightarrow{\phi} = -g\mathbf{M}\overrightarrow{\eta}$$

or

$$\begin{pmatrix} \mathbf{M} & 0 \\ 0 & \mathbf{M} \end{pmatrix} \partial_t \begin{pmatrix} \overrightarrow{\eta} \\ \overrightarrow{\phi} \end{pmatrix} = \begin{pmatrix} -\mathbf{B} & \mathbf{G} \\ -g\mathbf{M} & 0 \end{pmatrix} \begin{pmatrix} \overrightarrow{\eta} \\ \overrightarrow{\phi} \end{pmatrix} + \begin{pmatrix} \mathbf{B}\overrightarrow{G_1} \\ 0 \end{pmatrix}. \tag{A.17}$$

with $\overrightarrow{G_1}(t)$ is the influx signal vector at the boundary.

### A.2.2 Test Cases

#### A.2.2.1 Simulation on Uniform Mesh

Uniform mesh here means that all the quadrilaterals have uniform shape and are perfect rectangles. For the computational domain, the width and the length of the domain are $100km$, the number of elements is $100 \times 100$, the depth is $1km$, and the gravitational constant is $9.81m/s^2$. Hard wall boundary condition will be used here. First, we will give the initial condition as a single Gaussian hump in the middle of the domain, with initial potential velocity is zero everywhere. The wave will spread over the domain and when hit the wall, they will bounce back to the middle and so forth, since the mass and energy is conserved. The initial condition is shown is fig. (A.2), and pictures of the wave propagation can be seen in fig. (A.3). The energy conservation can be seen in fig. (A.4). The energy at the start of the simulation is $7.70476 \times 10^8$ $J$ and at the end is $7.70473 \times 10^8$ $J$.

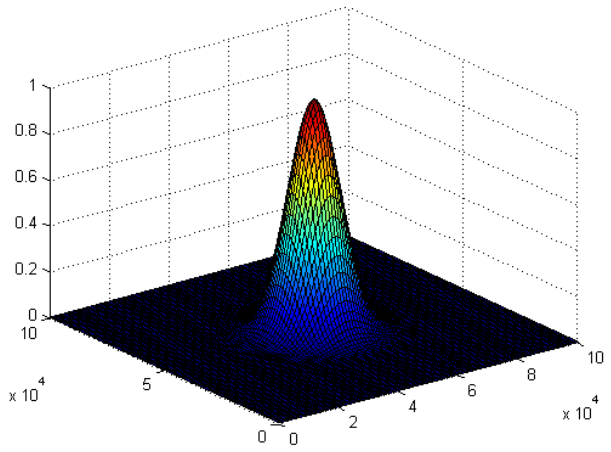


**Figure A.2:** Initial condition single Gaussian hump

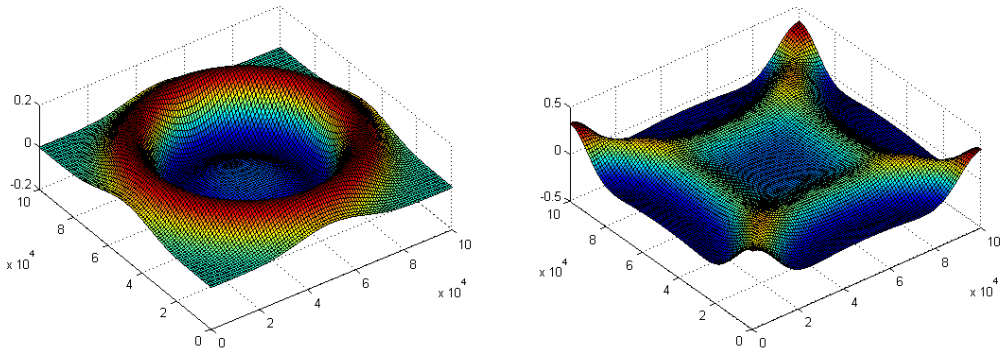


**Figure A.3:** Wave propagation at $t = 6min$ (left) $t = 12min$ (right

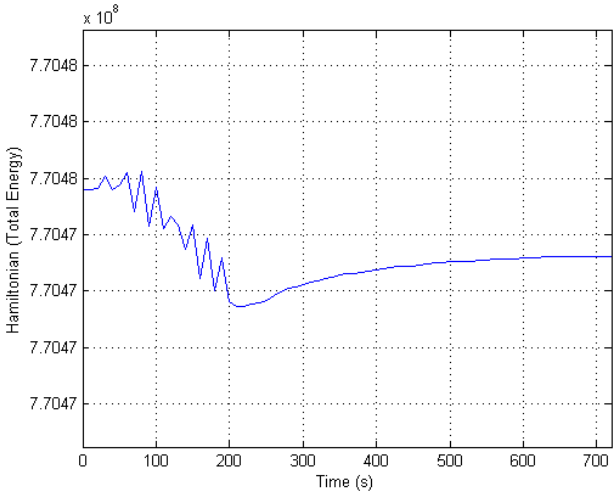


**Figure A.4:** Plot of energy conservation during the simulation

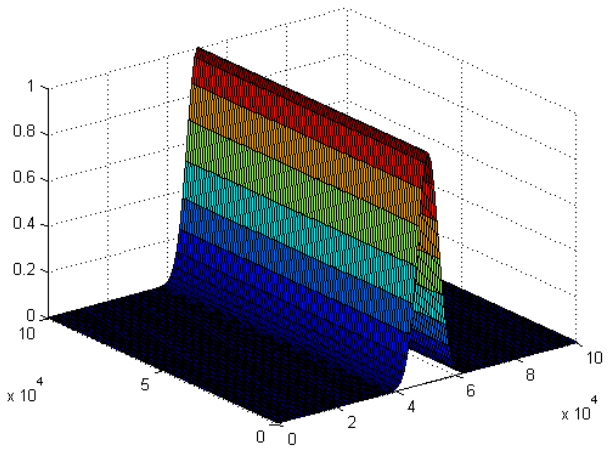


**Figure A.5:** Uniform sinusoidal function along $y$-axis as the initial condition

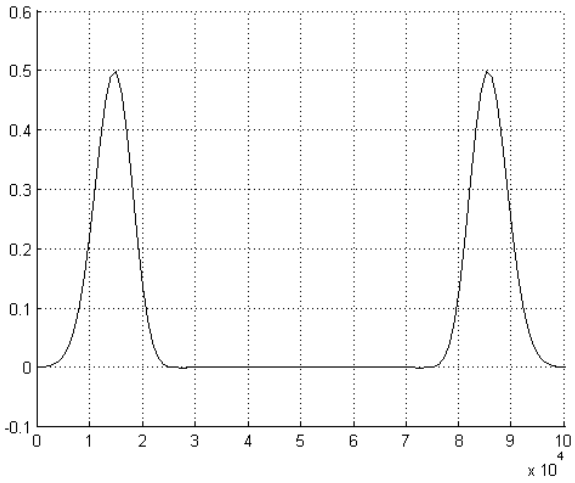


**Figure A.6:** Wave propagation at $t = 6min$

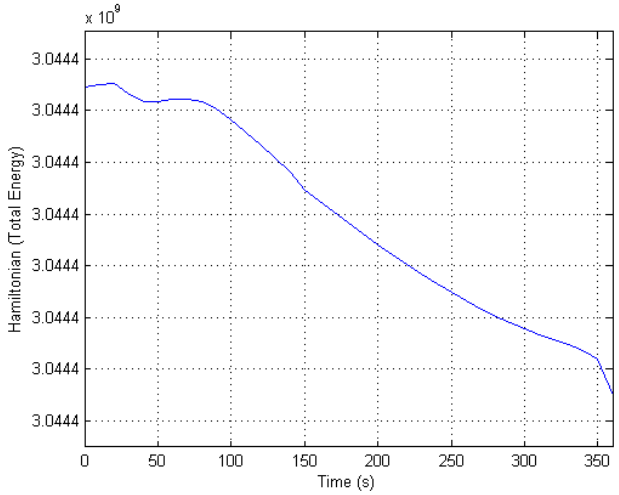


**Figure A.7:** Plot of energy conservation during the wave propagation

The second initial condition is uniform sinusoidal function along $y$-axis, with potential velocity is zero everywhere. Transparent boundary condition is used here. The analytical solution of this initial value problem is the wave will propagate to the left and to the right with the same form and half of the initial condition. The initial condition can be seen in fig. (A.5). Fig. (A.6) is the wave propagation at $t = 6min$. We can see that the wave height is half of the initial condition. We also can check our code through the group velocity of the wave. Since the depth is $1km$, then the wave velocity should be $\sqrt{9.81 \times 1000} = 99.0454m/s$. We can see that at $t = 6min$, the wave already about $35km$ from the initial condition. The energy conservation can be seen in fig. (A.7). The energy at the start of the simulation is $3.04441 \times 10^9$ $J$ and at the end is $3.04439 \times 10^9$ $J$.

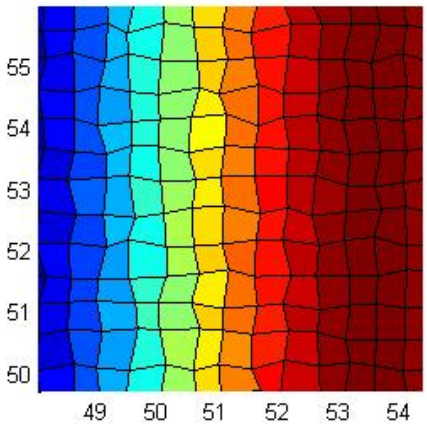


**Figure A.8:** Non-uniform (jiggled) mesh

#### A.2.2.2 Simulation on Non-uniform (jiggled) Mesh

Results of the simulation using uniform mesh has already shown that the code run well, but we still have to do the simulation using non-uniform mesh to make sure that all the transformation is run well. This is needed since some terms in the determinant of the Jacobian (A.8) will be zero when the element is a perfect rectangle. In fig (A.8), we can see the illustration of jiggled mesh used in the simulation.

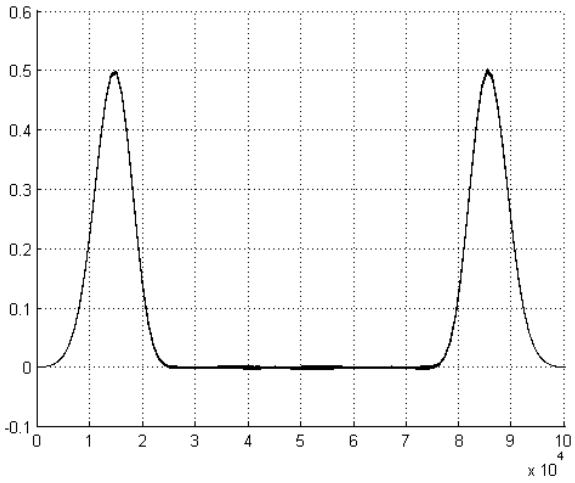


**Figure A.9:** Wave propagation at $t = 6min$

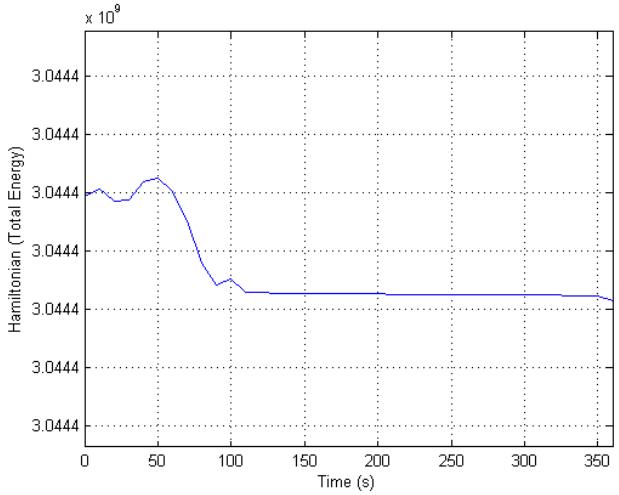


**Figure A.10:** Plot of energy conservation during the simulation

We will do the simulation again with the uniform sinusoidal function along $y-$axis as the initial condition (fig. (A.5)), and with velocity is zero everywhere. The boundary condition is transparent. Fig. (A.9) is the wave propagation at $t = 6min$. We can see that fig. (A.9) is almost the same with fig. (A.6). In fig. (A.9), there is 'thick' line between two propagated wave, and also at some points. This result is estimated as the consequence of using non-uniform mesh. In fig. (A.10), we can see the plot of energy conservation, which at the beginning of the simulation is $3.04442 \times 10^9$ $J$ and at the end is $3.04442 \times 10^9$ $J$.

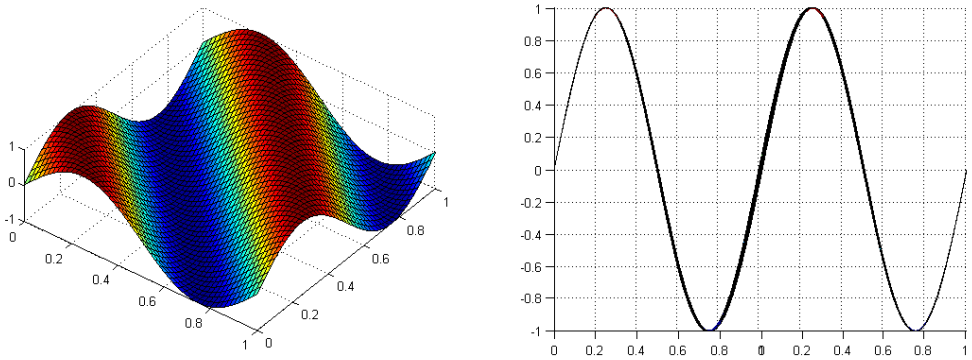

**Figure A.11:** Initial condition of harmonic waves

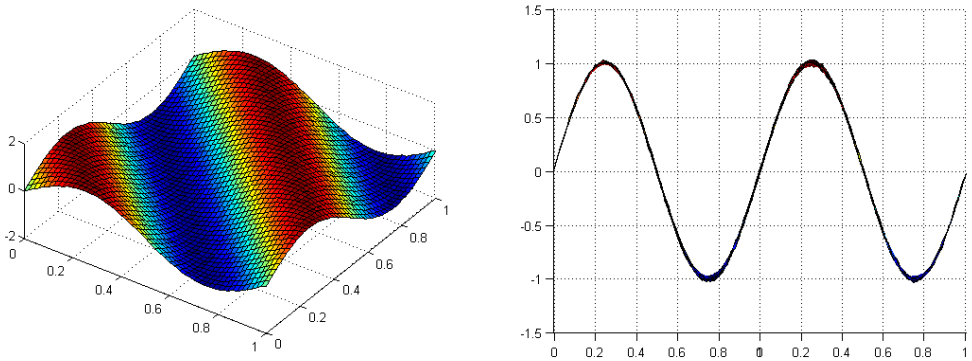

**Figure A.12:** Wave propagation of harmonic waves at $t = T$

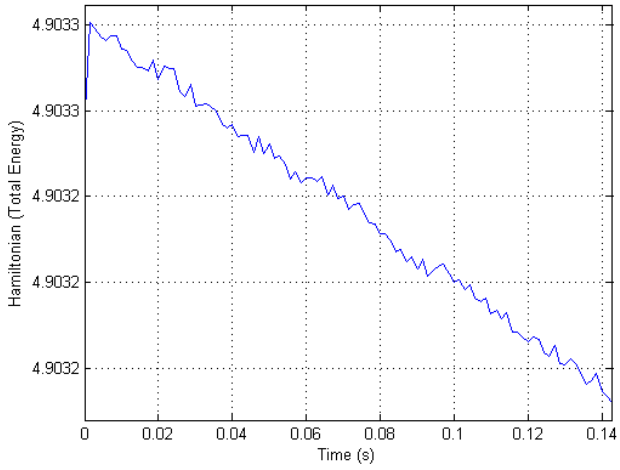


**Figure A.13:** Plot of energy conservation during the wave propagation

#### A.2.2.3 Harmonic waves

As the last simulation in linear SWE, we will do the test case using harmonic waves (using non-uniform mesh). The initial condition is given by

$$\eta(\mathbf{x}, 0) = A \sin(k_1 x + k_2 y) \tag{A.18}$$

$$\phi(\mathbf{x}, 0) = -\frac{g}{\omega} A \cos(k_1 x + k_2 y) \tag{A.19}$$

Then the period will be $T = \frac{2\pi}{\omega}$, with $\omega$ is the angular frequency defined as $\omega = k\sqrt{gh}$, and $k = \sqrt{k_1^2 + k_2^2}$ is the wave number (here, we will use $k_1 = k_2 = k_* = 2\pi$). As width and length of the domain, we will use the wavelength, which is defined as $\lambda = \frac{2\pi}{k_*}$. The number of elements is $50 \times 50$. For the simulation of harmonic waves, then we use the periodic boundary condition. Fig. (A.11) shows the plot of the initial condition, and fig (A.12) shows the wave propagation at $t = T$ (waves period). It can be seen that the waves profile is the same as the initial condition, as expected. After running the simulation for $20T$, we will get the energy (Hamiltonian plot) as fig (A.13), the energy at the beginning of the simulation is $4.90325J$ and at the end $4.90324J$. The $L^2 - error$ and $L^\infty - error$ of the wave elevation $\eta$ at $t = T$ on uniform grid can be seen in table (A.1).

| $N_x \times N_y$ | $h$ | $L^2 - error$ | $order$ | $L^\infty - error$ | $order$ |
|---|---|---|---|---|---|
| 8×8 | 0.125 | 0.0974 | - | 0.1554 | - |
| 16×16 | 0.0625 | 0.0224 | 2.12 | 0.0399 | 1.96 |
| 32×32 | 0.0313 | 0.0053 | 2.08 | 0.0103 | 1.95 |
| 64×64 | 0.0156 | 0.0013 | 2.03 | 0.0058 | 0.83 |

**Table A.1:** $L^2 - error$ and $L^\infty - error$ of the wave elevation $\eta$ at $t = T$ on uniform grid for linear SWE

## A.3 FEM Implementation for linear VBM

To get the solution of $\overrightarrow{\eta}$, $\overrightarrow{\phi}$, and $\overrightarrow{\psi}$ at each time step in (2.31)-(2.32), then we can use one of the methods to solve ordinary differential equations problem. Here, Runga Kutta method will be used. By using the Newton Cotes rule (A.9), then the approximation of $l_{ij}$ and $r_{ij}$ will be

$$l_{ij} \approx \frac{1}{4}\sum_{k=1}^{4}\left(-\frac{8}{15}h\nabla T_i \cdot \nabla T_j \left|J\right| - \frac{4}{3h}T_i T_j \left|J\right|\right)(\xi_k, \eta_k) \tag{A.20}$$

$$r_{ij} \approx \frac{1}{4}\sum_{k=1}^{4}(-\frac{2}{3}h\nabla T_i \cdot \nabla T_j \left|J\right|)(\xi_k, \eta_k) \ . \tag{A.21}$$

### A.3.1 FEM Implementation for Boundary Conditions

To implement VBM as wave models for tsunami simulation, we need boundary conditions. At this moment, we will use two types of boundary conditions, i.e. hardwall boundary condition (HBC) and periodic boundary condition (PBC).

#### A.3.1.1 Hardwall Boundary Condition

In the HBC, the normal flow through the boundary is assumed to be zero or $\mathbf{U}.\mathbf{n} = 0$, where $\mathbf{U}$ is fluid velocity. Note that we approximate the velocity potential at each depth by its value at the surface: $\Phi(\mathbf{x}, z, t) \approx \phi(\mathbf{x}, t)$, so the condition for hardwall can be rewritten as $\nabla\phi.\mathbf{n} = 0$ (since $U = \nabla_3\Phi$ and $\Phi \approx \phi$). The derivation of the governing equations of linear VBM from the first variation (2.24a)-(2.24c) do not give the corresponding boundary condition because the functional that we minimized accounts

only for the interior (from Pressure principle in (2.1)). We need to modify the weak formulation in order to incorporate the boundary conditions. Therefore, we use the corresponding governing equations from the weak formulation of (2.25a)-(2.25c) only for implementing the BC. To have the weak formulation of (2.25a)-(2.25c), we multiply the first equation of (2.25a)-(2.25c) by a test function and integrate it over a domain, then we do partial integration for the right hand side term, so we obtain the following equation for linear VBM

$$\int_{\Omega} v\partial_t \eta d\mathbf{x} = \int_{\Omega} h(\mathbf{x}) \bigtriangledown \phi . \bigtriangledown v d\mathbf{x} + \int_{\Omega} \beta(\mathbf{x}) \bigtriangledown \psi . \bigtriangledown v d\mathbf{x} \tag{A.22}$$

$$- \int_{\partial\Omega} \left(vh\left(\mathbf{x}\right) \bigtriangledown \phi.\mathbf{n}\right) d\partial\Omega - \int_{\partial\Omega} \left(v\beta\left(\mathbf{x}\right) \bigtriangledown \phi.\mathbf{n}\right) d\partial\Omega. \tag{A.23}$$

For HBC, the condition $\bigtriangledown\phi.\mathbf{n} = 0$ has to be satisfied in the boundary term(s) of (A.22). This condition makes the boundary term in (A.22) vanish. With this condition, we will have the system of matrix equation exactly the same with our system in (2.31)-(2.32). So the HBC's FEM implementation for VBM gives the same system of matrix equation as we derived based on the variational principle, when the BC term is ignored.

#### A.3.1.2 Periodic Boundary Condition

The Periodic Boundary Condition (PBC) in 2 dimensional case are

$$\eta(0, y, t) = \eta(L, y, t) \text{ and } \eta(x, 0, t) = \eta(H, 0, t) \tag{A.24a}$$

$$\phi(0, y, t) = \phi(L, y, t) \text{ and } \phi(x, 0, t) = \phi(H, 0, t) \tag{A.24b}$$

$$\psi(0, y, t) = \psi(L, y, t) \text{ and } \psi(x, 0, t) = \psi(H, 0, t) \tag{A.24c}$$

with $L$ is the length of the domain in $x-$direction and $H$ is the length of the domain in $y$-direction.

### A.3.2 Test Cases

For the linear VBM, we will do the same simulations as we did in linear SWE with non-uniform mesh. For the computational domain, the width and the length of the domain are $100m$, the number of elements is $100 \times 100$, the depth is $1km$, and the gravitational constant is $9.81m/s^2$. Hard wall boundary condition will be used here. First, with a single Gaussian hump in the middle of the domain, and the second with uniform sinusoidal function along $y-$axis, with initial potential velocity is zero everywhere. For the first case, fig. (A.14) shows us the propagation at $t = 6min$ and $t = 12min$. For the second case, fig. (A.15) is the wave propagation at $t = 6min$, in which we can see the dispersive effect of Linear VBM.

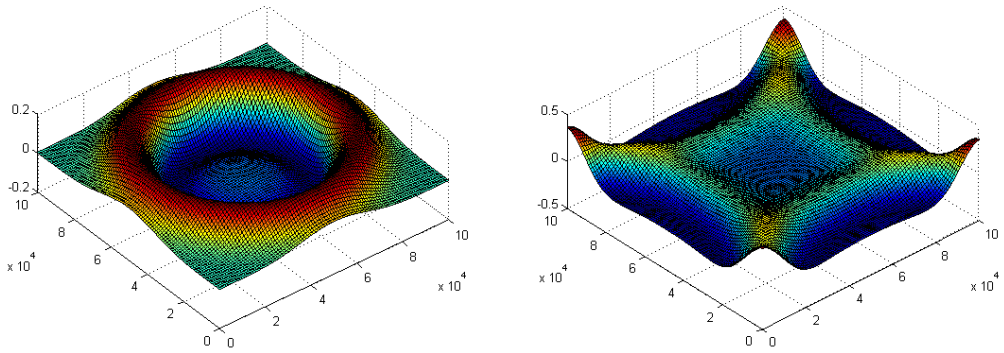


**Figure A.14:** Wave propagation at $t = 6min$ and $t = 12min$ (with a single Gaussian hump as initial condition)

#### A.3.2.1 Harmonic waves

By substitung the anzats $\eta = ae^{i(kx-\omega t)}, \phi = be^{i(kx-\omega t)}, \psi = ce^{i(kx-\omega t)}$ to (2.25c), we will get the dispersion relation of LVBM as

$$\omega^2 = ghk^2 \left(1 - \frac{\beta^2}{h} \frac{k^2}{\alpha k^2 + \gamma}\right). \tag{A.25}$$

First, we will use the initial condition:

$$\eta(\mathbf{x}, 0) = A \sin(k\mathbf{x})$$
$$\phi(\mathbf{x}, 0) = -\frac{g}{\omega} A \cos(k\mathbf{x})$$

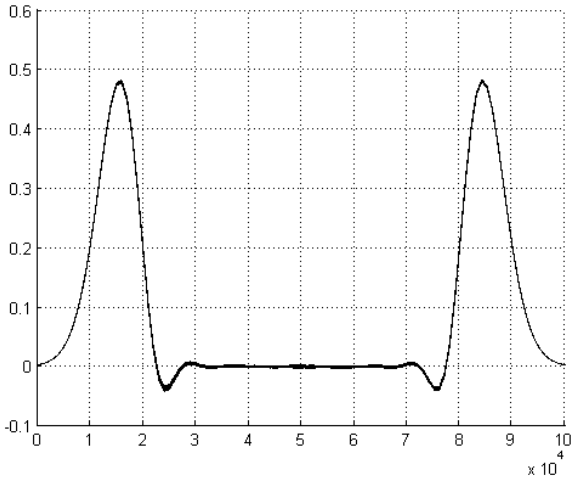


**Figure A.15:** Wave propagation at $t = 6min$ (with uniform sinusoidal along $y-$axis as initial condition)

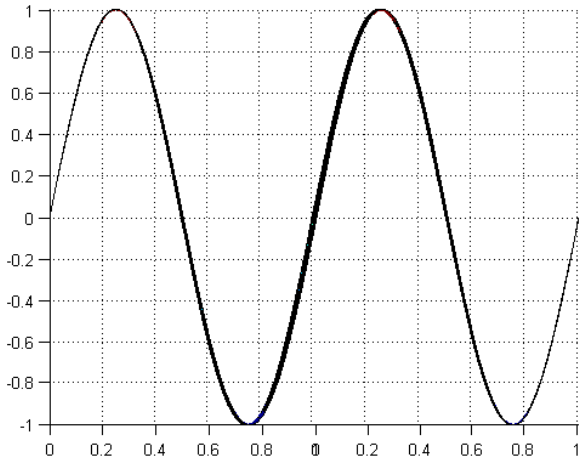


**Figure A.16:** Initial condition of harmonic waves

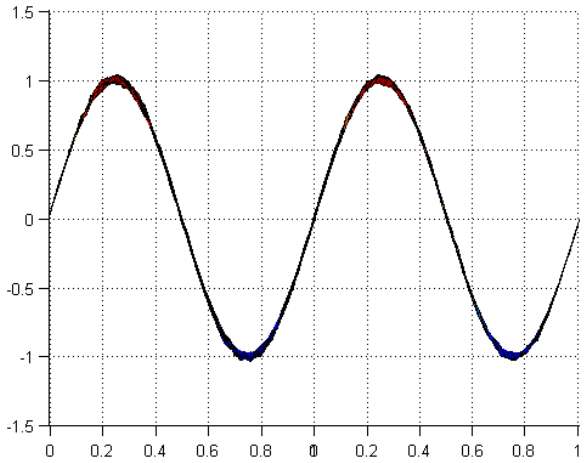


**Figure A.17:** Wave propagation of harmonic waves at $t = T$

with $k = 2\pi$. Fig (A.16) shows the initial condition, and fig (A.17) show the wave profile at $t = T = 2\pi/\omega$. The $L^2 - error$ and $L^\infty - error$ of the wave elevation $\eta$ at $t = T$ on uniform grid can be seen in table (A.2).

| $N_x \times N_y$ | $h$ | $L^2 - error$ | $order$ | $L^\infty - error$ | $order$ |
|---|---|---|---|---|---|
| 8×8 | 0.125 | 0.0974 | - | 0.1554 | - |
| 16×16 | 0.0625 | 0.0224 | 2.12 | 0.0399 | 1.96 |
| 32×32 | 0.0313 | 0.0053 | 2.08 | 0.0107 | 1.89 |
| 64×64 | 0.0156 | 0.0013 | 2.03 | 0.0053 | 1.01 |

**Table A.2:** $L^2 - error$ and $L^\infty - error$ of the wave elevation $\eta$ at $t = T$ on uniform grid for linear VBM

# A. NUMERICAL SOLUTION OF LINEAR SHALLOW WATER EQUATIONS AND LINEAR VARIATIONAL BOUSSINESQ MODEL

# Bibliography

[1] C. Cotter and O. Bokhove, A water wave model with horizontal circulation and accurate dispersion, *Memorandum 1896, Department of Applied Mathematics, University of Twente, Enschede*, 2009.

[2] E. van Groesen, Variational Boussinesq Model, part 1: Basic equations in Cartesian coordinates, *Technical Report of LabMath-Indonesia*, 2006.

[3] E. van Groesen and J. Molenaar, *Continuum Modeling in the Physical Sciences*, SIAM, 2007.

[4] E. J. Hinch, *Perturbation Methods*, Cambridge University Press, 1991.

[5] J. van Kan, F. Vermolen, and A. Segal, *Numerical Methods in Scientific Computing*, VSSD, 2006.

[6] G. Klopman, M. W. Dingemans, and E. van Groesen, A variational model for fully non-linear water waves of Boussinesq type, *Proc. 20th International Workshop on Water Waves and Floating Bodies*, 2005.

[7] J. C. Luke, A variational principle for fluids with a free surface, *J. Fluid Mech.* **27** (1967), 395.

[8] J. W. Miles, On Hamilton's principle for surface waves, *J. Fluid Mech.* **83** (1977), 153-158.

# Acknowledgements

This thesis is a final project report executed in the group of Mathematical Physics and Computational Mechanics, Department of Applied Mathematics, University of Twente and in LabMath-Indonesia. Here I would like to express my sincere thanks to the following people who have directly or indirectly involved in accomplishing this thesis.

First of all, Prof. E. van Groesen, for giving me the opportunity to study in The Netherlands, and for his patience to guide and supervise me in this research project. Next I would like to thank Dr. Onno Bokhove for all his criticism and straightforward manner, which teach me to become a better researcher. I would also like to thank Dr. Andonowati and Dr. Ardhasena Sopaheluwakan, for letting me doing part of this project in Labmath-Indonesia and for the sharing of their knowledge; and also Prof. Stephan van Gils for his willingness to be in the graduation committee.

I thank colleagues and friends within the MPCM group, especially for the member of 'Thursday informal meeting', Vijaya, Sander, Bob, Henk, Shavarsh, Masoumeh, Pak Tito, and Frank for the fruitful discussions. Also to Nida, Didit, Liam, and Ivan, for the waves discussions.

During the past two years here, in both good and difficult times, I am always encouraged by all my friends here in Enschede, in Indonesia, and somewhere in this world (through sms, email, messenger), so I never feel alone even during the work in the midnight. Special thanks to Pythia, Tettri, Ferry, Santy, Vero, Ola for all their support and willingness to listen me when I was down, and cheered me up again. To my new housemates, bang David and kak Vince, for the laughs in the last month of this thesis work;

we should do the 'sport' together more. I also thank my church friends, Maria, ce Shully, ce Santi, ko Yohan, ko Untung, also Pastor Widjaja and Tante Milka for all the counsels and continuous prayer.

I am very grateful to my brother and sister, Andri and Renny, for all their support and understanding. My special gratitude is directed to my late father and my mother, to whom this thesis is dedicated, for all their struggle for their children, and for their continuous prayer and unconditional love. For the completion of this thesis, I thank God for all His grace and blessings in my life.

*Enschede, August 2009*